HHS Public Access

Author manuscript

Nat Commun. Author manuscript; available in PMC 2015 August 27.

Published in final edited form as:

Nat Commun. ; 6: 6354. doi:10.1038/ncomms7354.

The Cholesterol Transporter ABCG1 Links Cholesterol Homeostasis and Tumor Immunity

Duygu Sag[1,*], **Caglar Cekic**[2,*], **Runpei Wu**[1], **Joel Linden**[3], and **Catherine C. Hedrick**[1]

[1]Division of Inflammation Biology, La Jolla Institute for Allergy and Immunology, La Jolla, CA 92037 USA

[2]Department of Molecular Biology and Genetics, Bilkent University 06800 Ankara, TURKEY

[3]Division of Developmental Immunology, La Jolla Institute for Allergy and Immunology, La Jolla, CA 92037 USA

Abstract

ATP-binding Cassette Transporter G1 (ABCG1) promotes cholesterol efflux from cells and regulates intracellular cholesterol homeostasis. Here, we demonstrate a role of ABCG1 as a mediator of tumor immunity. *Abcg1*$^{-/-}$ mice have dramatically suppressed subcutaneous MB49-bladder carcinoma and B16-melanoma growth and prolonged survival. We show that reduced tumor growth in *Abcg1*$^{-/-}$ mice is myeloid cell-intrinsic and is associated with a phenotypic shift of the macrophages from a tumor-promoting M2 to a tumor-fighting M1 within the tumor. *Abcg1*$^{-/-}$ macrophages exhibit an intrinsic bias toward M1 polarization with increased NF-κB activation and direct cytotoxicity for tumor cells *in vitro*. Overall, our study demonstrates that absence of ABCG1 inhibits tumor growth through modulation of macrophage function within the tumor and illustrates a link between cholesterol homeostasis and cancer.

INTRODUCTION

In addition to the cancer cells and their surrounding stroma, the tumor microenvironment contains innate and adaptive immune cells that can recognize and destroy tumors[1].

Corresponding Authors: Catherine C. Hedrick, Ph.D., Division of Inflammation Biology, La Jolla Institute for Allergy and Immunology, 9420 Athena Circle, La Jolla, CA 92037, hedrick@liai.org, Phone: 858-752-6500, Fax: 858-752-6985 and Duygu Sag, Ph.D., Division of Inflammation Biology, La Jolla Institute for Allergy and Immunology, 9420 Athena Circle, La Jolla, CA 92037, dsag@liai.org, Phone: 858-752-6620, Fax: 858-752-6985.

*Contributed equally

Postal address for Duygu Sag, Runpei Wu, Joel Linden and Catherine C. Hedrick: La Jolla Institute for Allergy and Immunology, 9420 Athena Circle, La Jolla, CA 92037 USA

Postal address for Caglar Cekic: Department of Molecular Biology and Genetics, Bilkent University, Faculty of Science, SB Building, 06800 Ankara, TURKEY

AUTHOR CONTRIBUTIONS

D.S and C.C designed and performed the experiments and analyzed the data; R.W provided technical assistance; J.L provided intellectual input, C.C.H and D.S. supervised the overall study and advised on study design and data interpretation; D.S and C.C.H wrote the manuscript.

COMPETING FINANCIAL INTERESTS

The authors declare no competing financial interests.

However, the tumor not only manages to evade the immune system through various mechanisms, but also it contrives to benefit from infiltrating immune cells by modifying their functions to create a microenvironment favorable to tumor progression[2]. Macrophages are major players of tumor immunity. Monocyte-derived macrophages can polarize into either M1 (classically activated) or M2 (alternatively activated) macrophage subtypes in the presence of specific polarization factors, including cytokines, growth factors and bioactive lipids, when recruited into peripheral tissues[3,4]. In general, M1 macrophages are potent tumor-fighting cells, whereas M2 macrophages display protumoral functions. The tumor recruits blood monocytes and promotes their differentiation mostly into M2-like macrophages[5]. M2-like tumor-associated macrophages (TAMs) play a key role in tumor growth and progression by producing molecules to promote angiogenesis, as well as survival and metastasis of tumor cells[6–9]. Moreover, TAMs affect adaptive immune responses by recruiting T regulatory cells (Tregs), which in turn suppress antitumor effector cells such as NK cells and $CD4^+$/$CD8^+$ T cells[10]. Several studies have reported a positive correlation between high TAM density and poor prognosis in human tumors, including bladder, breast and prostate[7,11]. Furthermore, it has been shown in different murine tumor models that either depletion of macrophages[12–16] or switching the phenotype of macrophages into tumor-fighting M1 macrophages[17–19] results in a significant reduction in tumor growth.

ATP-binding cassette transporter G1 (ABCG1) is a member of the ABC transporter family that regulates cellular cholesterol homeostasis[20]. Cholesterol homeostasis is crucial for survival and function of cells[21]. ABCG1 effluxes excess cholesterol from cells to high-density lipoprotein (HDL) particles for reverse cholesterol transport, which is the only path for elimination of cholesterol from the body[22,23]. ABCG1 is also important for the intracellular transport of cholesterol[24,25]. It is ubiquitously expressed in many cell types including, myeloid cells, lymphocytes and endothelial cells[20].

ABCG1 is known to regulate several aspects of macrophage biology. *Abcg1*$^{-/-}$ mice fed a Western-like diet display excessive lipid accumulation in macrophages[22]. Atherosclerosis studies demonstrated that ABCG1-deficient macrophages were more susceptible to apoptosis compared to wild-type macrophages under Western-like diet conditions *in vivo*[26,27]. Furthermore, *Abcg1*$^{-/-}$ macrophages have been shown to display enhanced pro-inflammatory cytokine production at basal level[28,29], in response to LPS[30] and when loaded with cholesterol[31]. ABCG1 also plays a role in T cell biology. We and others have reported that alterations in intracellular cholesterol homeostasis in the absence of ABCG1 increase proliferation of $CD4^+$ T cells[32,33] and impairs development of invariant natural killer T (*i*NKT) cells in thymus[34]. Overall, changes in cholesterol homeostasis by the absence of ABCG1 modulate immune cell function; however, the role of ABCG1 in anti-tumor immune responses is unknown.

In this study we demonstrate that *in vivo* deficiency of ABCG1 reduces tumor growth and increases survival of mice. Reduced tumor growth in the absence of ABCG1 is mediated through myeloid cell-intrinsic mechanisms and is associated with a shift of macrophages to a tumor fighting M1 phenotype within the tumor, which results in direct killing of tumor cells.

RESULTS

ABCG1-deficiency prevents tumor growth in mice

To determine if ABCG1 has an impact on tumor growth, MB49 bladder carcinoma or B16-F1 melanoma cells were first injected subcutaneously into 7–10 week old *Abcg1*$^{-/-}$ or control C57BL/6 (WT) mice fed a regular rodent chow diet (containing 0% cholesterol and 5% calories from fat) (Fig. 1a). Both groups of mice had comparable MB49 and B16-F1 tumor sizes when fed a chow diet (Fig. 1 b,c). Because ABCG1 regulates cholesterol homeostasis in the cell, to make the impact of ABCG1 deficiency more prominent, 7–10 week old *Abcg1*$^{-/-}$ and WT mice were next fed a Western-like diet (containing 0.2% cholesterol and 42% calories from fat) beginning a week before MB49 or B16-F1 tumor inoculation. The Western-like diet used in our studies is very similar in cholesterol and fat content to the typical Western-like diet chosen by many people in developed countries, and now increasingly in developing countries. *Abcg1*$^{-/-}$ mice fed a Western-like diet displayed dramatically reduced MB49 (4-fold at day 20) and B16-F1 (~3-fold at day 20) tumor growth compared to control mice (Fig. 1d,e). By 6–8 months of age, *Abcg1*$^{-/-}$ mice develop age-dependent phenotypes, such as pulmonary lipidosis and massive lipid deposition in macrophages[35] and these phenotypes are known to be accelerated by a Western-like diet[22]. Therefore, we also assessed the tumor growth in older (6–7 months old) *Abcg1*$^{-/-}$ and WT mice fed a chow diet. Interestingly, we found that aged *Abcg1*$^{-/-}$ mice when fed a chow diet had dramatically reduced MB49 tumor growth compared to aged-matched WT controls (Fig. 1f).

To investigate how Western-like diet affects the cholesterol profiles of tumor-bearing *Abcg1*$^{-/-}$ and WT mice, we performed FPLC analysis of plasma lipoprotein cholesterol profiles of MB49 tumor-bearing (day 12) 7–10 week old *Abcg1*$^{-/-}$ and WT mice fed either chow or Western-like diets. In line with the published literature on *Abcg1*$^{-/-}$ mice[24,36], plasma lipoprotein cholesterol profiles of tumor-bearing *Abcg1*$^{-/-}$ and WT mice were similar. In addition, Western-like diet feeding increased plasma lipoprotein cholesterol levels in both groups of mice (Fig. 1g). To further investigate the impact of ABCG1 deficiency on tumor progression, we crossed *Abcg1*$^{-/-}$ mice with apoE-deficient (*ApoE*$^{-/-}$)[37,38] and LDL-receptor deficient mice (*Ldlr*$^{-/-}$)[39,40]. The *ApoE*$^{-/-}$ and *Ldlr*$^{-/-}$ models are two hypercholesterolemic mouse models that are widely used to study atherosclerosis. Both genotypes have high plasma cholesterol levels when fed a chow diet and show profoundly increased plasma cholesterol levels when fed a Western-like diet[37–41]. We first compared plasma lipoprotein cholesterol profiles of MB49 tumor-bearing (day 12) 7–10 week old *Abcg1*$^{-/-}$ *ApoE*$^{-/-}$ mice with *ApoE*$^{-/-}$ mice and *Abcg1*$^{-/-}$ *Ldlr*$^{-/-}$ mice with *Ldlr*$^{-/-}$ mice, all fed a chow diet. We found that the loss of ABCG1 had no impact on plasma lipoprotein profiles in tumor-bearing hypercholesterolemic mice (Supplementary Fig. 1). We next measured subcutaneous tumor growth in *Abcg1*$^{-/-}$ mice crossed with these hypercholesterolemic mouse models. Interestingly, both 7–10 week old *Abcg1*$^{-/-}$ *Ldlr*$^{-/-}$ and *Abcg1*$^{-/-}$ *ApoE*$^{-/-}$ chow-fed mice showed dramatically reduced MB49 tumor growth compared to chow-fed control *Ldlr*$^{-/-}$ and *ApoE*$^{-/-}$ mice, respectively (Fig. 1h). Both genotypes also displayed a profound reduction in tumor growth when fed a Western-like diet (Fig. 1i,j). Collectively, these data show that Western-like diet feeding or crossing with

hypercholesterolemic mice is necessary to observe the changes in tumor growth in young *Abcg1*$^{-/-}$ mice, while this tumor phenotype is evident in aged *Abcg1*$^{-/-}$ mice fed a chow diet.

To investigate the impact of ABCG1 deficiency on spontaneous tumor metastasis, we utilized luciferase-expressing B16-F10 cells (B16-F10-luc2). B16-F10-luc2 cells were injected subcutaneously into Western-like diet-fed *Abcg1*$^{-/-}$ or WT mice. B16-F10-luc2 tumors grew aggressively and by day 28, the difference in tumor growth between *Abcg1*$^{-/-}$ and WT mice was significant, but not very prominent (Supplementary Fig. 2). This aspect of B16-F10-luc2 tumor growth allowed us to choose mice for study that had similar-sized tumors. Lungs from mice with similar, but average, tumor sizes in both groups were analyzed for spontaneous metastases of B16-F10 melanoma by bioluminescence imaging *ex vivo* (Supplementary Fig. 2). Subcutaneous B16 transplants have been shown to spontaneously metastasize to lung[42,43]. *Abcg1*$^{-/-}$ mice had significantly diminished tumor metastasis compared to WT mice (Supplementary Fig. 2). Subsequently, we examined the impact of ABCG1 deficiency on survival of tumor bearing mice. MB49 tumor-bearing *Abcg1*$^{-/-}$ mice showed prolonged survival compared to WT mice when fed a Western-like diet (Fig. 1k). Collectively, these data demonstrate that *in vivo* deficiency of ABCG1 impairs tumor growth and increases animal survival.

Reduced tumor growth in *Abcg1*$^{-/-}$ mice is immune-mediated

To determine if the impact of ABCG1 deficiency on tumor growth is mediated by immune cells, we used a bone marrow chimera approach. We measured MB49 tumor growth in Western-like diet-fed irradiated CD45.1^{+} B6.SJL (WT) mice, which were reconstituted with CD45.2^{+} *Abcg1*$^{-/-}$ or CD45.1^{+} B6.SJL bone marrow (Fig. 2a). WT mice reconstituted with *Abcg1*$^{-/-}$ bone marrow had a significant reduction in tumor growth over time compared to WT mice reconstituted with WT bone marrow (Fig. 2b), demonstrating that the impact of ABCG1 deficiency on tumor growth is immune cell-mediated.

The tumor microenvironment contains innate and adaptive immune cells, which display pro or anti-tumor functions. While NK cells, M1 macrophages, CD4^{+} Th1 cells and CD8^{+} T have been shown to act as tumor fighting cells, M2 macrophages and Tregs in tumor are known to support tumor progression. Dendritic cells (DCs), neutrophils and NKT cells have been shown to exert both tumor-suppressive and -promoting effects[1,44]. Next, we wanted to define the primary immune cell populations in the tumor microenvironment that are affected by the absence of ABCG1 under Western-like diet conditions. MB49 tumor cells were injected subcutaneously into either Western-like diet-fed or chow diet-fed *Abcg1*$^{-/-}$ and WT mice and tumor-infiltrating immune cells were analyzed by flow cytometry (For gating strategy see Supplementary Fig. 3). We found that the frequencies of macrophages and Tregs significantly decreased, whereas the frequencies of NK cells, CD4^{+} T cells and CD8^{+} T cells significantly increased in the tumors of Western-like diet-fed *Abcg1*$^{-/-}$ mice compared to WT mice (Fig. 2c). No significant differences were observed in the frequencies of tumor-infiltrating neutrophils, DCs or NKT cells in chow diet-fed or Western-like diet-fed *Abcg1*$^{-/-}$ or WT mice (Fig. 2c). These results demonstrate that ABCG1 deficiency

changes the balance between tumor promoting and tumor fighting immune cells within the tumor microenvironment.

Reduced tumor growth in *Abcg1*$^{-/-}$ mice is myeloid cell-intrinsic

To determine which cell type(s) were intrinsically affected by the absence of ABCG1 to impact tumor growth, we deleted ABCG1 selectively in either myeloid cells or T cells using Cre/loxP technology. We generated conditional knockout mice (*Abcg1*$^{fl/fl}$) in which *loxP* sites flank the Walker domain of exon 3 of *Abcg1* and crossed them with either LysM-Cre or Lck-Cre mice for selective deletion of ABCG1 in myeloid cells and T cells, respectively[45,46]. We observed ~95 % deletion of ABCG1 in macrophages from *Abcg1*$^{fl/fl}$-LysM-Cre^{+} mice and 70% deletion of ABCG1 in T cells from *Abcg1*$^{fl/fl}$-Lck-Cre^{+} mice (Supplementary Fig. 4).

We[32] and others[33] have previously reported that ABCG1 deficiency increases proliferation of CD4^{+} T cells. Therefore, it is possible that the impact of ABCG1 deficiency on tumor growth might be mediated directly through T cell-intrinsic mechanisms. To determine the impact of selective ABCG1 deletion in T cells on tumor growth, we injected MB49 tumor cells subcutaneously into Western-like diet-fed *Abcg1*$^{fl/fl}$-Lck-Cre^{+} and control *Abcg1*$^{fl/fl}$-Lck-Cre^{-} mice. The tumor growth in the *Abcg1*$^{fl/fl}$-Lck-Cre^{+} mice was comparable to control (Fig. 3a), indicating that the inhibition of tumor growth in the absence of ABCG1 is not mediated directly through T cells. However, we found that the tumor growth in *Abcg1*$^{fl/fl}$-LysM-Cre^{+} mice, which have selective ABCG1 deletion in myeloid cells, was dramatically reduced compared to control *Abcg1*$^{fl/fl}$-LysM-Cre^{-} mice (Fig. 3b). These data indicate that the reduced tumor growth in the absence of ABCG1 is mediated directly through myeloid cell intrinsic mechanisms.

Subsequently, we analyzed the tumor-infiltrating immune cells in MB49 tumors from Western-like diet-fed *Abcg1*$^{fl/fl}$-LysM-Cre^{+} and control mice by flow cytometry. In line with the changes in the frequencies of tumor-infiltrating immune cells in Western-like diet-fed *Abcg1*$^{-/-}$ mice (Fig. 2c), the frequencies of tumor-infiltrating macrophages and Tregs in *Abcg1*$^{fl/fl}$-LysM-Cre^{+} mice were significantly lower, whereas the frequencies of NK cells and CD4^{+} T cells were significantly higher compared to control (Fig. 3c). The frequencies of neutrophils, DCs, CD8^{+} cells and NKT cells in *Abcg1*$^{fl/fl}$-LysM-Cre^{+} mice and control mice were comparable (Fig. 3c). We also analyzed activation markers on tumor infiltrating immune cells. We observed that the mean fluorescence intensity (MFI) of CD69 expression on NK cells was significantly higher in *Abcg1*$^{fl/fl}$-LysM-Cre^{+} mice compared to control (Fig. 3d). The MFI of CD69 expression on CD4^{+} T cells, CD8^{+} T cells and NKT cells, the MFI of CD86 expression on macrophages and DCs, and the MFI of CD11b expression on neutrophils were similar between both genotypes (Fig. 3d). LysM-Cre mice have been shown to display Cre-mediated deletion of loxP-flanked target genes in myeloid cells; mainly in macrophages and neutrophils and partially in DCs[46]. In both Western-like diet-fed *Abcg1*$^{-/-}$ mice and *Abcg1*$^{fl/fl}$-LysM-Cre^{+} mice, the frequency of macrophages was decreased; whereas, no significant differences were observed in the frequencies or the activation of tumor-infiltrating neutrophils and DCs (Fig. 2c; 3c,d). Therefore, our data

suggest that ABCG1 deficiency in macrophages likely promotes multiple anti-tumor immune responses.

Impact of ABCG1-deficiency on apoptosis of tumor macrophages

Next, we investigated why ABCG1 deficiency caused a reduction in the frequency of macrophages in tumors. We first measured the frequency of monocytes in blood and in tumors from *Abcg1*$^{fl/fl}$-LysM-Cre^{+} and *Abcg1*$^{fl/fl}$-LysM-Cre^{-} mice fed a Western-like diet. The frequencies of monocytes in blood and tumors were similar in both groups (Fig. 4a), so changes in monocyte levels was not the cause. To determine if the reduction in the frequency of macrophages is due to an increase in macrophage cell death, we measured apoptosis of *Abcg1*$^{-/-}$ and WT macrophages in the tumor by Annexin V staining and flow cytometry. We found that the percentage of apoptotic (Annexin V^{+} live) macrophages in Western-like diet-fed *Abcg1*$^{-/-}$ mice was significantly higher compared to WT mice (Fig. 4b,c). The percentage of apoptotic macrophages in chow diet-fed *Abcg1*$^{-/-}$ and WT mice was comparable (Fig. 4d,e). These data show that macrophages in the tumor of *Abcg1*$^{-/-}$ mice fed a Western-like diet display increased apoptosis.

Abcg1$^{-/-}$ macrophages shift towards an M1 phenotype in the tumor

Excess cholesterol is exported out of the cell by the cholesterol transporters ABCG1 and ABCA1[47,48]. ABCG1 effluxes cholesterol to HDL particles[23]; while, ABCA1 promotes cholesterol efflux to lipid-poor apolipoprotein AI (apoAI)[49]. We found that *Abcg1*$^{-/-}$ macrophages expressed higher levels of *Abca1* compared to WT macrophages in the tumor (Supplementary Fig. 5). Subsequently, we investigated the phenotype of *Abcg1*$^{-/-}$ macrophages in the tumor. We analyzed the expression of CD11c, which is an M1-associated marker in tumor macrophages[50]. We found that in Western-like diet-fed *Abcg1*$^{-/-}$ mice, the percentage of F4/80^{high}CD11c^{high} (M1-like) macrophages was approximately 5 times higher than F4/80^{high}CD11c^{dim} (M2-like) macrophages, whereas in WT mice the percentages of both groups were similar (Fig. 5a,b). All the CD11c^{high} macrophages were also MHC II^{high} (data not shown). Moreover, we found that in chow diet-fed *Abcg1*$^{-/-}$ mice, the percentage of F4/80^{high}CD11c^{high} (M1-like) macrophages was only slightly (23%) higher than F4/80^{high}CD11c^{dim} (M2-like) macrophages, whereas in WT mice the percentages of both groups were similar (Supplementary Fig. 6). This shows that although *Abcg1*$^{-/-}$ macrophages display a slight shift towards an M1 phenotype (based on CD11c^{high}) even under chow diet conditions, this phenotypic shift becomes much more prominent when the mice were fed with Western-like diet. To further analyze the polarization phenotype of tumor macrophages in *Abcg1*$^{-/-}$ mice, we evaluated using quantitative real-time PCR (qPCR) the expression of M1 markers *Tnfα* and *Nos2* and M2 markers *Arg1*, *Ccl22 and Mrc1* in macrophages sorted via flow cytometry from tumors from Western-like diet-fed *Abcg1*$^{-/-}$ and WT mice. We found that the expression of *Tnfα* and *Nos2* was significantly higher in tumor macrophages from *Abcg1*$^{-/-}$ mice (Fig. 5c); whereas, the expression of *Arg1*, *Ccl22* and *Mrc1* was significantly lower in *Abcg1*$^{-/-}$ macrophages compared to WT macrophages (Fig. 5d). These data point to a shift in the phenotype of macrophages in the tumors of *Abcg1*$^{-/-}$ mice from tumor-promoting M2 macrophages to tumor-fighting M1 macrophages under Western-like diet conditions.

We also analyzed macrophages in spleens and lungs of Western-like diet-fed MB49 tumor-bearing *Abcg1*$^{-/-}$ and WT mice by flow cytometry at day 20. We found that *Abcg1*$^{-/-}$ alveolar macrophages displayed enhanced MHC II expression compared to control, suggesting an M1 skewing. This result is consistent with the previous studies, which reported that *Abcg1*$^{-/-}$ macrophages exhibited elevated proinflammatory activity in lung[28,29]. Although the level of MHC II expression in *Abcg1*$^{-/-}$ spleen macrophages tended to be higher compared to control, it did not reach statistical significance (Supplementary Fig. 7).

Next, we investigated why ABCG1-deficient macrophages shift towards an M1 phenotype in the tumor. Since we showed that *Abcg1*$^{-/-}$ macrophages from Western-like diet-fed mice displayed increased apoptosis compared to WT macrophages (Fig. 4b,c), one possible explanation of this M1 shift could be that *Abcg1*$^{-/-}$ M2 macrophages are more prone to apoptosis than *Abcg1*$^{-/-}$ M1 macrophages. To test this, we measured apoptosis of both M1 and M2 macrophages in tumors from Western-like diet-fed *Abcg1*$^{fl/fl}$-LysM-Cre^{+} and *Abcg1*$^{fl/fl}$-LysM-Cre^{-} mice by Annexin V staining and flow cytometry. We found that M1 and M2 tumor macrophages from *Abcg1*$^{fl/fl}$-LysM-Cre^{+} mice displayed similarly enhanced levels of apoptosis compared to control mice (Fig. 5e). Similar results for apoptosis were obtained also with staining for active Caspase-3 (Supplementary Fig. 8). These data indicate that the shift towards M1 phenotype in the tumor upon ABCG1 deficiency is not the result of M2 macrophages being more prone to apoptosis.

Next, we examined if *Abcg1*$^{-/-}$ macrophages are intrinsically biased toward M1 polarization. To test this, we generated bone marrow-derived macrophages (BMDMs) from *Abcg1*$^{-/-}$ and WT mice and polarized them to either an M1 phenotype by IFNγ/LPS stimulation or to an M2 phenotype by IL-4 stimulation *in vitro*. First, we measured *Abcg1* and *Abca1* mRNA expression in polarized WT BMDMs. Both IFNγ/LPS and IL-4 stimulation significantly increased *Abcg1* expression, but decreased *Abca1* expression in WT macrophages (Supplementary Fig. 9). Next, we determined the expression of M1 and M2 markers in polarized *Abcg1*$^{-/-}$ and WT BMDMs. We found that *Abcg1*$^{-/-}$ macrophages had increased production of the M1 markers TNFα (50%) and nitric oxide (50%) after IFNγ/LPS stimulation compared to control (Fig. 5f). Moreover, *Abcg1*$^{-/-}$ macrophages displayed enhanced expression of the M1 activation marker proteins MHC II (2.1 fold) and CD86 (~50%) when stimulated with the M1 inducers IFNγ/LPS (Fig. 5f). In contrast, *Abcg1*$^{-/-}$ macrophages displayed decreased expression of the M2 markers *Arg1* (2 fold), *Mrc1* (40%) and *Retnla* (Fizz1) (2.3 fold) after stimulation with the M2 inducer IL-4 (Fig. 6g). *Arg1* (~20 fold) and *Mrc1* (~2 fold) expression levels were also significantly lower in non-polarized (unstimulated) *Abcg1*$^{-/-}$ macrophages (Fig. 5g). These data indicate that *Abcg1*$^{-/-}$ macrophages exhibit an intrinsic bias toward M1 polarization. Altogether, these data show that the M1 shift of the *Abcg1*$^{-/-}$ macrophages in the tumor is not due to increased apoptosis of M2 macrophages, but rather that *Abcg1*$^{-/-}$ macrophages are biased toward M1 polarization.

Abcg1$^{-/-}$ macrophages accumulate cholesterol and cholesterol derivatives, such as 7-ketocholesterol (7-KC)[22,51]. To investigate if cholesterol and cholesterol derivatives have any impact on the M1 phenotype in macrophages, we incubated WT BMDMs with

cholesterol and other sterols, including 7α-hydroxycholesterol (7α-OHC), 25-hydroxycholesterol (25-OHC), 27-hydroxycholesterol (27-OHC), desmosterol, and 7-ketocholesterol (7-KC). After that, we either polarized BMDMs to an M1 phenotype by IFNγ/LPS stimulation or left them unstimulated. We found that incubation with cholesterol or 7-KC increased the levels of M1 markers, MHC II and TNFα in unstimulated macrophages. Incubation with cholesterol, but not 7-KC, also increased the levels of MHC II and TNFα after IFNγ/LPS stimulation (Fig. 6a,b). Incubation with 7α-OHC, 25-OHC, 27-OHC or desmosterol did not significantly alter the expression of M1 markers in either unstimulated or IFNγ/LPS- stimulated macrophages (data not shown). Thus, wild-type macrophages display an increase in the levels of M1 markers when incubated with cholesterol or 7-ketocholesterol, suggesting that the M1-bias in *Abcg1*$^{-/-}$ macrophages is likely due to the accumulation of these sterols.

To better understand why *Abcg1*$^{-/-}$ macrophages exhibit an intrinsic bias toward M1 polarization, we examined the activation of the transcription factor NF-κB, which is well-established as playing a critical role in the induction of pro-inflammatory gene expression in macrophages[52]. Phosphorylation of p65 subunit of NF-κB helps stabilize NF-κB in the nucleus for gene transcription[53] and thereby is widely used as an indicator of NF-κB activation. We evaluated the levels of NF-κB p65 (Ser-529) phosphorylation in unstimulated *Abcg1*$^{-/-}$ and WT BMDMs by flow cytometry. *Abcg1*$^{-/-}$ macrophages showed a ~50% higher level of p65 phosphorylation compared to WT macrophages (Fig. 6c,d), indicating that absence of ABCG1 results in increased NF-κB activation in macrophages, which is a likely cause for the observed M1 phenotype bias.

Abcg1$^{-/-}$ macrophages display enhanced tumor cytotoxicity

Next, we investigated how the shift of macrophages towards an M1 phenotype in the absence of ABCG1 reduces tumor growth. M2-like TAMs support tumor growth through various mechanisms including promoting angiogenesis[6–9] Therefore, ABCG1-deficiency might decrease the ability of macrophages to promote tumor angiogenesis. To test this, we assessed expression levels of endothelial cell markers in tumors from *Abcg1*$^{fl/fl}$-LysM-Cre^{+} and *Abcg1*$^{fl/fl}$-LysM-Cre^{-} mice by flow cytometry. We found comparable levels of CD45^{-} CD31^{+} CD34^{+} vascular endothelial cells in tumors from both mice groups (Fig. 7a,b), indicating that ABCG1-deficient macrophages are similar to WT macrophages in terms of promoting tumor angiogenesis, making this an unlikely mechanism.

Unlike M2-like TAMs, M1 macrophages can be cytotoxic to tumor cells, and in this way, can prevent tumor growth[54]. To investigate if the impact of ABCG1 deficiency on tumor growth can be through increased ability of macrophages to kill tumor cells directly, we performed an *in vitro* cytotoxicity assay. Briefly, we polarized bone marrow derived *Abcg1*$^{-/-}$ and WT macrophages to M1 phenotype by IFNγ/LPS stimulation and co-cultured these M1 macrophages with MB49 tumor cells. We assessed the viability of tumor cells by flow cytometry. We found that the frequency of dead tumor cells (CD45^{-} F4/80^{-} 7AAD^{+}) was 40% higher when they were co-cultured with *Abcg1*$^{-/-}$ macrophages, compared to WT macrophages (Fig. 7c,d). This indicates that *Abcg1*$^{-/-}$ macrophages display enhanced

cytotoxicity for tumor cells, making this a likely explanation for the reduced tumor growth observed *in vivo*.

DISCUSSION

In this study, we identify a novel role for the cholesterol transporter ABCG1 as a modulator of tumor immunity. The absence of ABCG1 inhibits tumor growth through modulation of macrophage survival and phenotype within the tumor. Collectively, our data demonstrate an important new concept that cholesterol homeostasis in immune cells can determine the outcome of tumor growth *in vivo*.

LysM-Cre mice have been shown to display Cre-mediated deletion of loxP-flanked target genes in myeloid cells; mainly in macrophages and neutrophils and partially in DCs[46]. In tumors from Western-like diet-fed *Abcg1*$^{-/-}$ mice and *Abcg1*$^{fl/fl}$-LysM-Cre^{+} mice, the frequency of macrophages was reduced; while, the frequencies and the activation of neutrophils and DCs were similar compared to control (Fig. 2c; 3c,d). Moreover, we showed that ABCG1-deficient macrophages exhibit an intrinsic bias toward tumor-fighting M1 polarization and display enhanced ability to kill tumor cells directly (Fig. 7c,d). Therefore, we conclude that the reduced tumor growth in the absence of ABCG1 is mediated through macrophage-intrinsic mechanisms.

Increased apoptosis of *Abcg1*$^{-/-}$ macrophages was also reported in atherosclerosis studies in mice, in which increased numbers of apoptotic macrophages were found within atherosclerotic lesions of Western-like diet-fed *Abcg1*$^{-/-}$ *ApoE*$^{-/-}$ mice and *Ldlr*$^{-/-}$ mice transplanted with *Abcg1*$^{-/-}$ bone marrow[26,27]. In addition, *Abcg1*$^{-/-}$ macrophages have been shown to undergo apoptosis after a challenge with oxLDL[26,51] *in vitro*. Increased apoptosis of ABCG1-deficient macrophages is a result of the accumulation of specific toxic oxysterols, including 7-ketocholesterol, which are known to induce apoptosis[27,51]. 7-ketocholesterol and related oxysterols have been shown to be selectively exported out of the cell by ABCG1, but not by ABCA1[51]. Furthermore, the observed shift of *Abcg1*$^{-/-}$ macrophages in the tumor towards a proinflammatory M1 phenotype (Fig. 5a–d) is in concordance with a previous study in atherosclerosis, which reported that macrophages from *Abcg1*$^{-/-}$ mice fed a Western-like/high-cholesterol diet exhibited elevated proinflammatory activity[31]. Macrophages are known to accumulate cholesterol in the absence of ABCG1[22]. Our data demonstrate that macrophages display an increase in the levels of M1 markers when incubated with cholesterol or 7-ketocholesterol (Fig. 6a,b), suggesting that the M1-bias in *Abcg1*$^{-/-}$ macrophages is likely due to the excess sterol accumulation. In addition, similar to a previous report, which showed enhanced content of nuclear NF-κB p65 in *Abcg1*$^{-/-}$ peritoneal macrophages after LPS stimulation[30], we observed elevated NF-κB p65 phosphorylation in *Abcg1*$^{-/-}$ BMDMs (Fig. 6c,d). A previous study by Li *et al.* reported that free cholesterol accumulation in macrophages induced production of proinflammatory cytokines through activation of IκB kinase/NF-κB pathway[55]. Therefore, based on our data we surmise that increased cholesterol accumulation in macrophages in the absence of ABCG1 causes NF-κB activation, which polarizes these macrophages to a proinflammatory/tumor-fighting M1 phenotype. M1 macrophages produce TNFα and NO, which can mediate cytolysis of tumor cells[54]. Thus, enhanced production of TNFα and NO in *Abcg1*$^{-/-}$ M1

macrophages that we reported here (Fig. 5c,f) is likely the cause of the observed increase in direct cytotoxicity of *Abcg1*$^{-/-}$ macrophages for tumor cells (Fig. 7c,d).

In most tumor models, the majority of the macrophages in tumors display a tumor-promoting M2 phenotype[5]. Our study shows that ABCG1-deficiency not only reduces the number of macrophages within the tumor, but also causes a shift of the remaining macrophages to a tumor-fighting M1 phenotype. Therefore, ABCG1 may constitute a therapeutic target for cancer.

TAMs can promote tumor growth by different mechanisms. Production of CCL22 by immunosuppressive TAMs has been shown to recruit tumor-promoting Tregs to the tumor site[10]. Thus, our observation of reduced Treg frequency in the tumor in the absence of ABCG1 could be explained by a reduction in the frequency of TAMs (Fig. 2c,3c) and a phenotypic shift of the remaining TAMs to M1 macrophages, which are not potent CCL22 producers (Fig. 5c,d). Tregs suppress expansion of anti-tumor effector cells including NK cells and CD4$^+$ T cells[10]. Therefore, our observation of an increase in the frequency of NK cells and CD4$^+$ T cells in the absence of ABCG1 could be explained by a decrease in the frequency of Tregs in the tumor (Fig. 2c; 3c). Our data support the notion that M1 phenotypic shift of *Abcg1*$^{-/-}$ macrophages with reduced CCL22 production results in reduced Treg recruitment, which in turn increases tumor infiltration by NK cells and CD4$^+$ T cells. Since, these cells are well-established tumor fighting cells[1], an increase in their frequency would have an impact on tumor growth. Collectively, our data support the concept that absence of ABCG1 in macrophages drives changes in macrophage-intrinsic cytokine production and as such, could increase NK cell and CD4$^+$ T cell infiltration into the tumor to further prevent tumor growth.

Our study suggests that intrinsic loss of ABCG1 in macrophages is of critical importance for the mechanisms behind the effects on tumor growth. Our data support the notion that accumulation of cholesterol in macrophages in the absence of ABCG1 impacts their survival and phenotype, thus, changing their function in the tumor. Since *Abcg1*$^{-/-}$ macrophages cannot efflux cholesterol properly, more cholesterol accumulates in *Abcg1*$^{-/-}$ macrophages compared to WT macrophages, which has been well-documented[22]. In young *Abcg1*$^{-/-}$ mice, macrophage cholesterol accumulation is accelerated by Western-like diet feeding or by crossing the mice onto a hypercholesterolemic mouse model background. However, our finding that aged *Abcg1*$^{-/-}$ mice display reduced tumor growth when fed a chow diet supports the notion that macrophages in older *Abcg1*$^{-/-}$ mice accumulate more cholesterol over time[44]. Thus, in the aged *Abcg1*$^{-/-}$ mice, the tumor phenotype becomes evident even on a chow diet.

Enhanced expression of ABCG1 but reduced expression of ABCA1 after LPS/IFNγ or IL-4 stimulation in WT macrophages (Supplementary Fig. 9) point to an importance of ABCG1 in macrophage activation. Increased expression of ABCA1 in *Abcg1*$^{-/-}$ TAMs is not surprising (Supplementary Fig. 5), since we[32,34] and others[36,56] have previously shown that genetic deletion of one cholesterol transporter, either ABCG1 or ABCA1, is compensated for by an up-regulation of the other transporter. Nevertheless, neither ABCG1 nor ABCA1 can fully compensate for the loss of the other[20]. However, we cannot rule out the possibility

that changes in ABCA1 expression contributed to our observed findings of reduced tumor growth in *Abcg1*$^{-/-}$ mice. Future studies using ABCA1-deficient mice will be useful to delineate the roles of these two transporters in tumor immunity.

From many perspectives, atherosclerosis and cancer are fundamentally different. However, the immune system plays a major role in the progression of both diseases. Human population and animal studies clearly demonstrate that HDL protects against atherosclerosis[57]. Interestingly, meta-analysis of lipid-altering therapies has indicated an inverse relationship between plasma HDL levels and incidence of cancer[58]. In concordance with this report, a recent study has shown that apoAI, the major protein component of HDL, suppresses tumor growth and metastasis in mice via modulation of immune responses[59]. Collectively, these studies suggest that HDL has a role both in atherosclerosis and cancer. ABCG1 deficiency in immune cells has been shown to protect mice from atherosclerosis development[26,36]. By demonstrating that myeloid cell-specific ABCG1 deletion suppresses tumor growth, our present study suggests that ABCG1 might link immunity in atherosclerosis and cancer.

In sum, our study identifies ABCG1 as a novel mediator of anti-tumor immune responses. It defines an important role for cholesterol transporters in tumor immunity and provides a link between lipid homeostasis and cancer. Understanding how ABCG1 and cholesterol metabolism in immune cells impacts anti-tumor immune responses could lead to development of entirely new therapeutic approaches for cancer immunotherapy.

METHODS

Mice

C57BL/6J mice (000664), *Ldlr*$^{-/-}$ mice (002207) and *ApoE*$^{-/-}$ mice (002052) were purchased from The Jackson Laboratory (Bar Harbor, ME). *Abcg1*$^{-/-}$*/lacZ* knock-in mice were purchased from Deltagen (San Mateo, CA) and are congenic to a C57BL/6J background (backcrossed 14 generations). B6.SJL-Ptprca/BoyAiTac mice (CD45.1 congenic, 004007) were purchased from Taconic Farms (Germantown, NY). *Abcg1*$^{-/-}$ mice were crossed with *Ldlr*$^{-/-}$ and *ApoE*$^{-/-}$ mice to obtain *Abcg1*$^{-/-}$ *Ldlr*$^{-/-}$ and *Abcg1*$^{-/-}$*ApoE*$^{-/-}$ mice, respectively. Conditional knockout *Abcg1*$^{fl/fl}$ mice (C57BL/6J background) in which loxP sites flank the Walker domain of exon 3 of *Abcg1* were generated for our laboratory using InGenious Targeting Laboratory (New York). A ~10.3 kb region used to construct the targeting vector was first subcloned from a positively identified BAC clone using homologous recombination. The region was designed such that the short homology arm (SA) extends 2.2 kb 5' to lox P/FRT flanked Neo cassette. The long homology arm (LA) ends on the 3' side of lox P/FRT flanked Neo cassette and is ~ 8.1 kb long. The single lox P site is inserted upstream of exon 3, and the lox P/FRT-flanked Neo cassette is inserted downstream of exon 3. The target region is 1.5 kb including exon 3. The targeting vector is confirmed by restriction analysis after each modification step and by sequencing using primers designed to read from the selection cassette into the 3' end of the LA (N7) and the 5' end of the SA (N1), or from primers that anneal to the vector sequence, P6 and T7, and read into the 5' and 3' ends of the BAC sub clone. *Abcg1*$^{fl/fl}$ mice were crossed with Lck-Cre mice (003802, The Jackson Laboratory) to obtain *Abcg1*$^{fl/fl}$-Lck-Cre^{+}

and control *Abcg1*$^{fl/fl}$-Lck-Cre^{-} mice; and crossed with LysM-Cre mice (004781 , The Jackson Laboratory) to obtain *Abcg1*$^{fl/fl}$-LysM-Cre^{+} and *Abcg1*$^{fl/fl}$-LysM-Cre^{-} mice. All the mice used in this study were female and 7–10 weeks old, except for the tumor growth experiment in the aged *Abcg1*$^{-/-}$ and C57BL/6 (WT) mice, which were 6–7 months old. Mice were fed a standard rodent chow diet containing 0% cholesterol and 5% calories from fat (Pico lab, #5053) or Western-like diet containing 0.2% cholesterol and 42% calories from fat (Harlan Laboratories, #TD88137). The mice were housed in microisolator cages in a pathogen-free animal facility of the La Jolla Institute for Allergy and Immunology.

The plasma lipid profile analyses were performed at day 12, because this is the very earliest time that significant differences were observed in tumor growth. Day 12 is also the time when differences in macrophage apoptosis were observed, which then later on leads to a more prominent difference in tumor growth. Tumor growth was measured till days 18–20 and that is the time when the frequency and phenotype of the immune cells within the tumor were analyzed.

All experiments followed guidelines of the La Jolla Institute for Allergy and Immunology Animal Care and Use Committee and approval for use of rodents was obtained from the La Jolla Institute for Allergy and Immunology according to criteria outlined in the Guide for the Care and Use of Laboratory Animals from the National Institutes of Health. Mice were euthanized by CO_2 inhalation.

Cell lines and reagents

MB49 bladder carcinoma and B16-F1 melanoma cells were derived from C57BL/6 mice and obtained from American Type Culture Collection. The B16-F10-luc2 cell line was established by Caliper Life Sciences by transduction of lentivirus containing luciferase 2 gene under the control of human ubiquitin C promoter. Tumor cells were cultured in R5 medium containing RPMI 1640, 5% heat-inactivated FBS, 50 U/ml penicillin and 50 μg/ml streptomycin. Cells were injected into mice after reaching 60–80% confluency.

Flow cytometry antibodies including anti-mouse APC-F4/80 (BM8) (1/100), FITC-Ly6G (RB6-8C5) (1/200), APC/Cy7 or AF700-CD45 (30-F11) (1/200), AF700-CD45.2 (104) (1/200), PerCP/Cy5.5-NK1.1 (PK136) (1/100), e-Fluor 450-CD4 (RM4-5) (1/200), FITC-TCRβ (H57-597) (1/400), PE-CD25 (PC61.5) (1/100), APC-Foxp3 (FJK-16s) (1/100), AF700-CD34 (RAM34) (1/200) and e-Fluor 450-MHC II (M5/114.15.2) (1/200), were purchased from eBioscience (San Diego, CA); PE-Cy7-CD11b (M1/70) (1/800), PE-CD11c (HL3) (1/300), FITC-CD45.1 (A20) (1/200), APC/Cy7-CD8α (53–6.7) (1/200), PE-Cy7-CD69 (H1.2F3) (1/400), PE-CD31 (MEC 13.3) (1/300) and PE-phospho-p65 (S529) (K10-895.12.50) (1/10), were purchased from BD Biosciences (San Jose, California); PerCP/Cy5.5-CD19 (6D5) (1/100), PE-CD115 (AFS98) (1/100) and AF700-CD86 (GL-1) (1/200) were purchased from Biolegend (San Diego, CA). CD16/CD32 (2.4G2) (1/200) antibody was purchased from BD Biosciences. Ultrapure LPS (*Escherichia coli* 0111:B4) was purchased from InvivoGen (San Diego, CA), murine rIFNγ and rIL-4 were purchased from R&D Systems (Minneapolis, MN), murine M-CSF was purchased from PeproTech (Rocky Hill, NJ) and RPMI 1640 medium was purchased from Invitrogen (Carlsbad, CA). FBS, Collagenase IV, water-soluble cholesterol, 7α-hydroxycholesterol, 25-

hydroxycholesterol, 27-hydroxycholesterol, desmosterol and 7-ketocholesterol were purchased from Sigma-Aldrich (St. Louis, MO). DNase I was purchased from Roche (Basel, Switzerland), PBS was purchased from Thermo Scientific (Rockford, IL) and Ficoll-Paque™ plus was purchased from GE Healthcare (Pittsburgh, PA).

Measurement of tumor growth/metastasis and survival

10^5 MB49 or B16-F1 cells in 100 μl PBS were injected subcutaneously into the right flanks of female age-matched 7–10 weeks old *Abcg1*$^{-/-}$, C57BL/6 (WT), *Abcg1*$^{-/-}$ *Ldlr*$^{-/-}$, *Ldlr*$^{-/-}$, *Abcg1*$^{-/-}$*ApoE*$^{-/-}$, *ApoE*$^{-/-}$, *Abcg1*$^{fl/fl}$-Lck-Cre^{+}, *Abcg1*$^{fl/fl}$-Lck-Cre^{-}, *Abcg1*$^{fl/fl}$-LysM-Cre^{+} and *Abcg1*$^{fl/fl}$- LysM-Cre $^{-}$ mice or 6–7 months old *Abcg1*$^{-/-}$ and WT mice. Mice were fed with either Western-like diet or chow diet beginning a week before injection of tumor cells. Tumor diameters were measured using a digital caliper and tumor volume was calculated using the formula $V = D \times d^2/2$, where V is the tumor volume, D is the largest measured tumor diameter and d is the smallest measured tumor diameter. For the survival experiments, the mice with tumor volume reaching 2000 mm^3 were sacrificed and considered as dead. To measure spontaneous lung metastasis, 10^5 luciferase expressing B16-F10 cells (B16-F10-luc2) in 100 μl PBS were injected into female age-matched *Abcg1*$^{-/-}$ and C57BL/6 mice subcutaneously. Mice were fed with Western-like diet beginning a week before injection of tumor cells. B16-F10-luc2 tumors grow more aggressively than B16-F1 tumors which allowed us to choose mice for study that had similar-sized tumors. At 28 days after B16-F10-luc2 tumor inoculation, mice with similar, but average, tumor sizes in both groups were anesthetized by inhalation of isoflurane (Butler Animal Health Supply) and 1 mg D-Luciferin (Caliper Life Sciences, Waltham, MA) in 100 μL PBS was delivered into each mouse retro-orbitally. Mice were sacrificed 2 min after D-Luciferin injection, lungs were harvested and lung metastases were measured using an IVIS 200 Bioluminescence Imager (Caliper Life Sciences, Hopkinton, MA).

Measurement of plasma lipoproteins

Mice were fed with either chow diet or Western-like diet beginning a week before injection of tumor cells. Blood (in EDTA) was collected from chow diet-fed or Western-like diet-fed mice 12 days after MB49 tumor inoculation. Plasma lipoprotein profiles were obtained by fast protein liquid chromatography (FPLC) as described previously[60,61]. Briefly, equal volumes of plasma from 5 mice per group were pooled and 200 μl of this pooled plasma was applied to a set of 2 Superose 6 (HR 10/30) columns linked in series. Lipoproteins were eluted by size exclusion into 0.5 ml fractions in EDTA/NaCl/NaN3 (1 mmol/L; 0.154 mol/L; 0.02%) at a flow rate of 0.5 mL/min. Cholesterol was measured in each fraction using an enzymatic cholesterol kit (Wako) according to manufacturers' instructions.

Generation of bone marrow chimeras

Recipient B6.SJL mice were irradiated in two doses of 500 rad each (for a total of 1000 rad) 4 h apart. Bone marrow cells from both femurs and tibias of B6.SJL (CD45.1) and *Abcg1*$^{-/-}$ (CD45.2) donor mice were collected under sterile conditions. Bones were centrifuged for the collection of marrow, cells were washed and resuspended in PBS for injection. 10^7 bone marrow cells from B6.SJL or *Abcg1*$^{-/-}$ mice in 200 μl PBS were delivered retro-orbitally

into each recipient mouse. Recipient mice were housed in a barrier facility under pathogen-free conditions and were provided autoclaved acidified water with antibiotics (trimethoprim-sulfamethoxazole) and were fed autoclaved food. The chimeric mice were fed with Western-like diet starting 6 weeks after bone marrow reconstitution.

Flow cytometry

Tumors were meshed through a 100-μm strainer (Fisher Scientific, Pittsburg, PA) and then filtered through a 40-μm strainer. Single cell suspension was resuspended in 100 μl flow cytometry staining buffer (1% BSA plus 0.1% sodium azide in PBS). Fcγ receptors were blocked with CD16/32 blocking antibody for 10 min and surface antigens on cells were stained for 30 min at 4 °C. LIVE/DEAD Fixable Dead Cell Stain (Invitrogen) was used for analysis of viability, and forward- and side-scatter parameters were used for exclusion of doublets from analysis. Antibody clones and dilutions used are listed above. For intracellular staining, cells were fixed and permeabilized with the Cytofix/Cytoperm Fixation/ Permeabilization Solution Kit (BD Biosciences) (for cytoplamis proteins) or Foxp3 Staining Buffer Set (eBioscience) (for nuclear proteins) after the cell surface staining. Cells were stained with directly conjugated fluorescent of Foxp3 antibody for 30 min at 4 °C and with directly conjugated fluorescent of NF-κB phospho-p65 (Ser 529) antibody for 30 min at RT. Apoptosis of macrophages in tumor was measured by flow cytometry using a PE Annexin V Apoptosis Detection Kit 1 or a FITC active Caspase-3 Apoptosis Kit (BD Biosciences) according to the manufacturer's instructions. Cell fluorescence was assessed using LSR-II (BD Biosciences) and data were analyzed with FlowJo software (TreeStar, Ashland, OR). Macrophages ($CD45^+$, $NK1.1^-$, $Ly6G^-$, $CD11b^+$, $F4/80^{high}$), neutrophils ($CD45^+$, $NK1.1^-$, $Ly6G^+$, $CD11b^+$), myeloid dendritic cells ($CD45^+$, $NK1.1^-$, $Ly6G^-$, $F4/80^-$, $CD11b^+$ $CD11c^+$), monocytes ($CD45^+$, $NK1.1^-$, $Ly6G^-$, $CD11b^+$, $CD115^+$), NK cells ($CD45^+$, $TCR\beta^-$, $NK1.1^+$), $CD4^+$ T cells ($CD45^+$, $TCR\beta^+$, $NK1.1^-$, $CD4^+$), $CD8^+$ T cells ($CD45^+$, $TCR\beta^+$, $NK1.1^-$, $CD8^+$), NKT cells ($CD45^+$, $TCR\beta^+$, $NK1.1^+$), Tregs ($CD45^+$, $TCR\beta^+$, $NK1.1^-$, $CD4^+$,$CD25^+$, $Foxp3^+$) were identified with the appropriate gating.

Cell sorting

Tumors from WT and *Abcg1*$^{-/-}$ mice at day 20 were enriched for $CD11b^+$ cells by positive selection with mouse $CD11b^+$ positive selection kit (Stem Cell Technologies, Vancouver, Canada) according to the manufacturer's instructions, before cell sorting. Surface antigens on enriched $CD11b^+$ cells were then stained as described above, followed by macrophage ($Ly6G^-$, $NK1.1^-$, $CD11b^+$, $F4/80^{high}$) sorting with a FACSAria cytometer (BD Biosciences). Peritoneal lavage from *Abcg1*$^{fl/fl}$-LysM-Cre^+ and *Abcg1*$^{fl/fl}$- LysM-Cre^- mice 5 days post thioglycollate injection was sorted for macrophages ($F4/80^{high}$) and splenocytes from *Abcg1*$^{fl/fl}$-Lck-Cre^+ and *Abcg1*$^{fl/fl}$-Lck-Cre^- mice were sorted for T cells ($CD3^+$) using FACSAria cytometer.

Tumor angiogenesis

Tumors were minced and digested with Collagenase IV (400 U/ml) in the presence of DNase I (20 μg/ml) in RPMI medium at 37 °C for 30 min. Cell suspension was filtered through a 40-μm strainer and resuspended in warm R5 medium and incubated at 37 °C for

30 min. The cells were stained with fluorophore-conjugated antibodies against CD45, CD31, CD34 and analyzed by flow cytometry.

Generation and M1/M2 polarization of BMDMs

Bone marrow-derived macrophages (BMDMs) were prepared as described previously[62,63]. Briefly, bone marrow cells were cultured in standard tissue culture plates in the presence of 10 ng/ml M-CSF overnight. Non-adherent cells from this initial culture were then transferred to low-attachment six-well plates (Corning Life Sciences, Tewksbury MA) in 4 ml R5 medium containing 30% L929 conditioned medium and 10 ng/ml M-CSF per well for 7 days, adding more medium on days 3 and 6. After that, the cells were purified by centrifugation over Ficoll-Paque™ plus. Cells were verified to be 98% $CD11b^+$, $F4/80^+$, MHC II^{low}, $CD80^{low}$, $CD86^{low}$ by flow cytometry.

WT and *Abcg1*$^{-/-}$ BMDMs were allowed to rest at 37 °C over night before stimulation. For M1 polarization, macrophages were either stimulated with IFNγ (20 ng/ml) for 12 hours followed by LPS (100 ng/ml) stimulation for 4 hours (for MHC II and CD86 analysis) or stimulated with IFNγ (20 ng/ml) + LPS (100 ng/ml) overnight (for TNFα and NO analysis). For M2 polarization, macrophages were stimulated with IL-4 (20 ng/ml) for 16 hours.

Stimulation of macrophages with cholesterol and -derivatives

WT bone marrow-derived macrophages were allowed to rest at 37 °C over night before stimulation. The next day, macrophages were pre-incubated with water-soluble cholesterol (20 μg/ml), 7α-hydroxycholesterol (1 μM), 25-hydroxycholesterol (1 μM), 27-hydroxycholesterol (1 μM), desmosterol (5 μM) or 7-ketocholesterol (5 μM) for 2 hours. Next, macrophages were either left unstimulated or stimulated with IFNγ (20 ng/ml) for 12 hours followed by LPS (100 ng/ml) stimulation for 4 hours (for MHC II analysis) or stimulated with IFNγ (20 ng/ml) + LPS (100 ng/ml) overnight (for TNFα analysis).

Cytokine and nitric oxide (NO) measurements

The supernatants were collected and TNFα was measured by ELISA (eBioscience) and NO (as nitrite) was measured by the Griess Reagent System (Promega, Madison, WI) according to the manufacturers' instructions.

In vitro tumor cytotoxicity assay

WT and *Abcg1*$^{-/-}$ bone marrow-derived macrophages were plated in round well 96-well plates as 4×10^5 cells/well in 200 μl R5 and stimulated with IFNγ (20 ng/ml) and LPS (100 ng/ml) for 24 hours. The cells were washed with R5 twice and co-cultured with 10^4 MB49 tumor cells (40:1 ratio of effector (macrophages): target cells (tumor cells)). 24 hours later, the cells were washed with PBS and treated with Accutase™ cell detachment solution (BD Biosciences). Tumor cell viability was determined with 7-AAD staining by flow cytometry. Tumor cytotoxicity was calculated as % of $7\text{-}AAD^+$ tumor cells ($CD45^-$, $F4/80^-$) co-cultured with macrophages ($CD45^+$, $F4/80^+$) - % $7\text{-}AAD^+$ of tumor cells alone.

Quantitative real-time PCR

Total cellular RNA of macrophages was collected with an RNeasy Plus Micro Kit according to the manufacturer's protocol (Qiagen, Valencia, CA). RNA purity and quantity was measured with a nanodrop spectrophotometer (Thermo Scientific). Approximately 500 ng RNA was used for synthesis of cDNA with an Iscript cDNA Synthesis Kit (Bio-Rad, Hercules, CA). Total cDNA was diluted 1:20 in H_2O, and a volume of 9 μl was used for each real-time condition with a MyIQ Single-Color Real-Time PCR Detection System (Bio-Rad) and TaqMan Gene Expression Mastermix and *Arg1* (# Mm00475988_m1), *Ccl22* (# Mm00436439_m1), *Mrc1* (# Mm00485148_m1),*Tnfa* (# Mm00443258_m1), *Rtnla* (# Mm00445109_m1), *Nos2* (# Mm00440502_m1), *Abcg1* (# Mm01348250_m1) and *Abca1* (# Mm01350760_m1) TaqMan primers (Applied Biosystems). Data were analyzed and presented on the basis of the relative expression method[64]. The formula for this calculation is as follows: relative expression = $2^{-(S\Delta\, Ct\, -\, C\Delta C\, t\,)}$ where ΔC_t is the difference in the threshold cycle between the gene of interest and the housekeeping gene (18S), S is the *Abcg1*$^{-/-}$ mouse, and C is the WT mouse.

Statistical analyses

Data for all experiments were analyzed with Prism software (GraphPad). Two-way ANOVA test, long-rank test, unpaired Student's t test and Wilcoxon-matched-pairs signed rank test were used for comparison of experimental groups when appropriate. The data shown are the means ± s.e.m. *P* values of less than 0.05 were considered statistically significant.

Supplementary Material

Refer to Web version on PubMed Central for supplementary material.

ACKNOWLEDGMENTS

We thank Amy Blatchley, Debbi Yoakum, Fernando Vazquez, Dr. Iftach Shaked, the Department of Laboratory Animal Care, and the Flow Cytometry Facility at the La Jolla Institute for Allergy and Immunology (LJI) for excellent technical assistance. We thank Dr. Gerhard Wingender and Dr. Klaus Ley at LJI for valuable scientific contributions. We also thank Jennifer Pattison and Dr. Joseph Witztum at University of California San Diego for assistance with plasma lipoprotein analysis. This work was supported by NIH R01 HL097368 (to C.C.H.) and NIH P01 HL55798 (to C.C.H.).

REFERENCES

1. Grivennikov SI, Greten FR, Karin M. Immunity, inflammation, and cancer. Cell. 140:883–899. [PubMed: 20303878]
2. Whiteside TL. The tumor microenvironment and its role in promoting tumor growth. Oncogene. 2008; 27:5904–5912. [PubMed: 18836471]
3. Mantovani A, Sica A, Locati M. Macrophage polarization comes of age. Immunity. 2005; 23:344–346. [PubMed: 16226499]
4. Martinez FO, Helming L, Gordon S. Alternative activation of macrophages: an immunologic functional perspective. Annu Rev Immunol. 2009; 27:451–483. [PubMed: 19105661]
5. Solinas G, Germano G, Mantovani A, Allavena P. Tumor-associated macrophages (TAM) as major players of the cancer-related inflammation. J Leukoc Biol. 2009; 86:1065–1073. [PubMed: 19741157]
6. Coussens LM, Werb Z. Inflammation and cancer. Nature. 2002; 420:860–867. [PubMed: 12490959]

7. Lewis CE, Pollard JW. Distinct role of macrophages in different tumor microenvironments. Cancer Res. 2006; 66:605–612. [PubMed: 16423985]
8. Mantovani A, Sozzani S, Locati M, Allavena P, Sica A. Macrophage polarization: tumor-associated macrophages as a paradigm for polarized M2 mononuclear phagocytes. Trends Immunol. 2002; 23:549–555. [PubMed: 12401408]
9. Pollard JW. Tumour-educated macrophages promote tumour progression and metastasis. Nat Rev Cancer. 2004; 4:71–78. [PubMed: 14708027]
10. Nishikawa H, Sakaguchi S. Regulatory T cells in tumor immunity. Int J Cancer. 127:759–767. [PubMed: 20518016]
11. Sica A, et al. Macrophage polarization in tumour progression. Semin Cancer Biol. 2008; 18:349–355. [PubMed: 18467122]
12. Hiraoka K, et al. Inhibition of bone and muscle metastases of lung cancer cells by a decrease in the number of monocytes/macrophages. Cancer Sci. 2008; 99:1595–1602. [PubMed: 18754872]
13. Lin EY, et al. Macrophages regulate the angiogenic switch in a mouse model of breast cancer. Cancer Res. 2006; 66:11238–11246. [PubMed: 17114237]
14. Lin EY, Nguyen AV, Russell RG, Pollard JW. Colony-stimulating factor 1 promotes progression of mammary tumors to malignancy. J Exp Med. 2001; 193:727–740. [PubMed: 11257139]
15. Miselis NR, Wu ZJ, Van Rooijen N, Kane AB. Targeting tumor-associated macrophages in an orthotopic murine model of diffuse malignant mesothelioma. Mol Cancer Ther. 2008; 7:788–799. [PubMed: 18375821]
16. Zeisberger SM, et al. Clodronate-liposome-mediated depletion of tumour-associated macrophages: a new and highly effective antiangiogenic therapy approach. Br J Cancer. 2006; 95:272–281. [PubMed: 16832418]
17. Colombo MP, Mantovani A. Targeting myelomonocytic cells to revert inflammation-dependent cancer promotion. Cancer research. 2005; 65:9113–9116. [PubMed: 16230363]
18. Guiducci C, Vicari AP, Sangaletti S, Trinchieri G, Colombo MP. Redirecting in vivo elicited tumor infiltrating macrophages and dendritic cells towards tumor rejection. Cancer research. 2005; 65:3437–3446. [PubMed: 15833879]
19. Ostrand-Rosenberg S, Grusby MJ, Clements VK. Cutting edge: STAT6-deficient mice have enhanced tumor immunity to primary and metastatic mammary carcinoma. Journal of immunology. 2000; 165:6015–6019.
20. Tarr PT, Tarling EJ, Bojanic DD, Edwards PA, Baldan A. Emerging new paradigms for ABCG transporters. Biochim Biophys Acta. 2009; 1791:584–593. [PubMed: 19416657]
21. Ikonen E. Cellular cholesterol trafficking and compartmentalization. Nat Rev Mol Cell Biol. 2008; 9:125–138. [PubMed: 18216769]
22. Kennedy MA, et al. ABCG1 has a critical role in mediating cholesterol efflux to HDL and preventing cellular lipid accumulation. Cell Metab. 2005; 1:121–131. [PubMed: 16054053]
23. Wang N, Lan D, Chen W, Matsuura F, Tall AR. ATP-binding cassette transporters G1 and G4 mediate cellular cholesterol efflux to high-density lipoproteins. Proc Natl Acad Sci U S A. 2004; 101:9774–9779. [PubMed: 15210959]
24. Sturek JM, et al. An intracellular role for ABCG1-mediated cholesterol transport in the regulated secretory pathway of mouse pancreatic beta cells. The Journal of clinical investigation. 2010; 120:2575–2589. [PubMed: 20530872]
25. Tarling EJ, Edwards PA. ATP binding cassette transporter G1 (ABCG1) is an intracellular sterol transporter. Proceedings of the National Academy of Sciences of the United States of America. 2011; 108:19719–19724. [PubMed: 22095132]
26. Baldan A, et al. Impaired development of atherosclerosis in hyperlipidemic Ldlr−/− and ApoE−/− mice transplanted with Abcg1−/− bone marrow. Arterioscler Thromb Vasc Biol. 2006; 26:2301–2307. [PubMed: 16888235]
27. Tarling EJ, et al. Impaired development of atherosclerosis in Abcg1−/− Apoe−/− mice: identification of specific oxysterols that both accumulate in Abcg1−/− Apoe−/− tissues and induce apoptosis. Arterioscler Thromb Vasc Biol. 30:1174–1180. [PubMed: 20299684]
28. Baldan A, Gomes AV, Ping P, Edwards PA. Loss of ABCG1 results in chronic pulmonary inflammation. J Immunol. 2008; 180:3560–3568. [PubMed: 18292583]

29. Wojcik AJ, Skaflen MD, Srinivasan S, Hedrick CC. A critical role for ABCG1 in macrophage inflammation and lung homeostasis. J Immunol. 2008; 180:4273–4282. [PubMed: 18322240]
30. Yvan-Charvet L, et al. Increased inflammatory gene expression in ABC transporter-deficient macrophages: free cholesterol accumulation, increased signaling via toll-like receptors, and neutrophil infiltration of atherosclerotic lesions. Circulation. 2008; 118:1837–1847. [PubMed: 18852364]
31. Yvan-Charvet L, et al. Combined deficiency of ABCA1 and ABCG1 promotes foam cell accumulation and accelerates atherosclerosis in mice. J Clin Invest. 2007; 117:3900–3908. [PubMed: 17992262]
32. Armstrong AJ, Gebre AK, Parks JS, Hedrick CC. ATP-binding cassette transporter G1 negatively regulates thymocyte and peripheral lymphocyte proliferation. J Immunol. 184:173–183. [PubMed: 19949102]
33. Bensinger SJ, et al. LXR signaling couples sterol metabolism to proliferation in the acquired immune response. Cell. 2008; 134:97–111. [PubMed: 18614014]
34. Sag D, et al. ATP-Binding Cassette Transporter G1 Intrinsically Regulates Invariant NKT Cell Development. Journal of immunology. 2012; 189:5129–5138.
35. Baldan A, et al. Deletion of the transmembrane transporter ABCG1 results in progressive pulmonary lipidosis. J Biol Chem. 2006; 281:29401–29410. [PubMed: 16887795]
36. Ranalletta M, et al. Decreased atherosclerosis in low-density lipoprotein receptor knockout mice transplanted with Abcg1−/− bone marrow. Arteriosclerosis, thrombosis, and vascular biology. 2006; 26:2308–2315.
37. Plump AS, et al. Severe hypercholesterolemia and atherosclerosis in apolipoprotein E-deficient mice created by homologous recombination in ES cells. Cell. 1992; 71:343–353. [PubMed: 1423598]
38. Zhang SH, Reddick RL, Piedrahita JA, Maeda N. Spontaneous hypercholesterolemia and arterial lesions in mice lacking apolipoprotein E. Science. 1992; 258:468–471. [PubMed: 1411543]
39. Ishibashi S, et al. Hypercholesterolemia in low density lipoprotein receptor knockout mice and its reversal by adenovirus-mediated gene delivery. The Journal of clinical investigation. 1993; 92:883–893. [PubMed: 8349823]
40. Ishibashi S, Goldstein JL, Brown MS, Herz J, Burns DK. Massive xanthomatosis and atherosclerosis in cholesterol-fed low density lipoprotein receptor-negative mice. The Journal of clinical investigation. 1994; 93:1885–1893. [PubMed: 8182121]
41. Ishibashi S, Herz J, Maeda N, Goldstein JL, Brown MS. The two-receptor model of lipoprotein clearance: tests of the hypothesis in "knockout" mice lacking the low density lipoprotein receptor, apolipoprotein E, or both proteins. Proceedings of the National Academy of Sciences of the United States of America. 1994; 91:4431–4435. [PubMed: 8183926]
42. Nathanson SD, Haas GP, Mead MJ, Lee M. Spontaneous regional lymph node metastases of three variants of the B16 melanoma: relationship to primary tumor size and pulmonary metastases. J Surg Oncol. 1986; 33:41–45. [PubMed: 3762173]
43. Stackpole CW. Intrapulmonary spread of established B16 melanoma lung metastases and lung colonies. Invasion Metastasis. 1990; 10:267–280. [PubMed: 2228515]
44. Swann J, Crowe NY, Hayakawa Y, Godfrey DI, Smyth MJ. Regulation of antitumour immunity by CD1d-restricted NKT cells. Immunol Cell Biol. 2004; 82:323–331. [PubMed: 15186264]
45. Hennet T, Hagen FK, Tabak LA, Marth JD. T-cell-specific deletion of a polypeptide N-acetylgalactosaminyl-transferase gene by site-directed recombination. Proceedings of the National Academy of Sciences of the United States of America. 1995; 92:12070–12074. [PubMed: 8618846]
46. Clausen BE, Burkhardt C, Reith W, Renkawitz R, Forster I. Conditional gene targeting in macrophages and granulocytes using LysMcre mice. Transgenic Res. 1999; 8:265–277. [PubMed: 10621974]
47. Gelissen IC, et al. ABCA1 and ABCG1 synergize to mediate cholesterol export to apoA-I. Arteriosclerosis, thrombosis, and vascular biology. 2006; 26:534–540.

48. Vaughan AM, Oram JF. ABCA1 and ABCG1 or ABCG4 act sequentially to remove cellular cholesterol and generate cholesterol-rich HDL. J Lipid Res. 2006; 47:2433–2443. [PubMed: 16902247]
49. Vedhachalam C, et al. Mechanism of ATP-binding cassette transporter A1-mediated cellular lipid efflux to apolipoprotein A-I and formation of high density lipoprotein particles. J Biol Chem. 2007; 282:25123–25130. [PubMed: 17604270]
50. Movahedi K, et al. Different tumor microenvironments contain functionally distinct subsets of macrophages derived from Ly6C(high) monocytes. Cancer research. 2010; 70:5728–5739. [PubMed: 20570887]
51. Terasaka N, Wang N, Yvan-Charvet L, Tall AR. High-density lipoprotein protects macrophages from oxidized low-density lipoprotein-induced apoptosis by promoting efflux of 7-ketocholesterol via ABCG1. Proc Natl Acad Sci U S A. 2007; 104:15093–15098. [PubMed: 17846428]
52. Karin M, Delhase M. The I kappa B kinase (IKK) and NF-kappa B: key elements of proinflammatory signalling. Semin Immunol. 2000; 12:85–98. [PubMed: 10723801]
53. Hu J, Nakano H, Sakurai H, Colburn NH. Insufficient p65 phosphorylation at S536 specifically contributes to the lack of NF-kappaB activation and transformation in resistant JB6 cells. Carcinogenesis. 2004; 25:1991–2003. [PubMed: 15192014]
54. Escorcio-Correia M, Hagemann T. Measurement of tumor cytolysis by macrophages. Curr Protoc Immunol. 2011 Chapter 14, Unit 14 18 11-11.
55. Li Y, et al. Free cholesterol-loaded macrophages are an abundant source of tumor necrosis factor-alpha and interleukin-6: model of NF-kappaB- and map kinase-dependent inflammation in advanced atherosclerosis. J Biol Chem. 2005; 280:21763–21772. [PubMed: 15826936]
56. Brunham LR, et al. Beta-cell ABCA1 influences insulin secretion, glucose homeostasis and response to thiazolidinedione treatment. Nature medicine. 2007; 13:340–347.
57. Rye KA, Bursill CA, Lambert G, Tabet F, Barter PJ. The metabolism and anti-atherogenic properties of HDL. J Lipid Res. 2009; 50(Suppl):S195–S200. [PubMed: 19033213]
58. Jafri H, Alsheikh-Ali AA, Karas RH. Baseline and on-treatment high-density lipoprotein cholesterol and the risk of cancer in randomized controlled trials of lipid-altering therapy. J Am Coll Cardiol. 2010; 55:2846–2854. [PubMed: 20579542]
59. Zamanian-Daryoush M, et al. The cardioprotective protein apolipoprotein A1 promotes potent anti-tumorigenic effects. J Biol Chem. 2013; 288:21237–21252. [PubMed: 23720750]
60. Castellani LW, et al. Overexpression of apolipoprotein AII in transgenic mice converts high density lipoproteins to proinflammatory particles. The Journal of clinical investigation. 1997; 100:464–474. [PubMed: 9218525]
61. Warden CH, Hedrick CC, Qiao JH, Castellani LW, Lusis AJ. Atherosclerosis in transgenic mice overexpressing apolipoprotein A-II. Science. 1993; 261:469–472. [PubMed: 8332912]
62. Cekic C, et al. MyD88-dependent SHIP1 regulates proinflammatory signaling pathways in dendritic cells after monophosphoryl lipid A stimulation of TLR4. Journal of immunology. 2011; 186:3858–3865.
63. Sag D, Carling D, Stout RD, Suttles J. Adenosine 5'-monophosphate-activated protein kinase promotes macrophage polarization to an anti-inflammatory functional phenotype. Journal of immunology. 2008; 181:8633–8641.
64. Livak KJ, Schmittgen TD. Analysis of relative gene expression data using real-time quantitative PCR and the 2(-Delta Delta C(T)) Method. Methods. 2001; 25:402–408. [PubMed: 11846609]

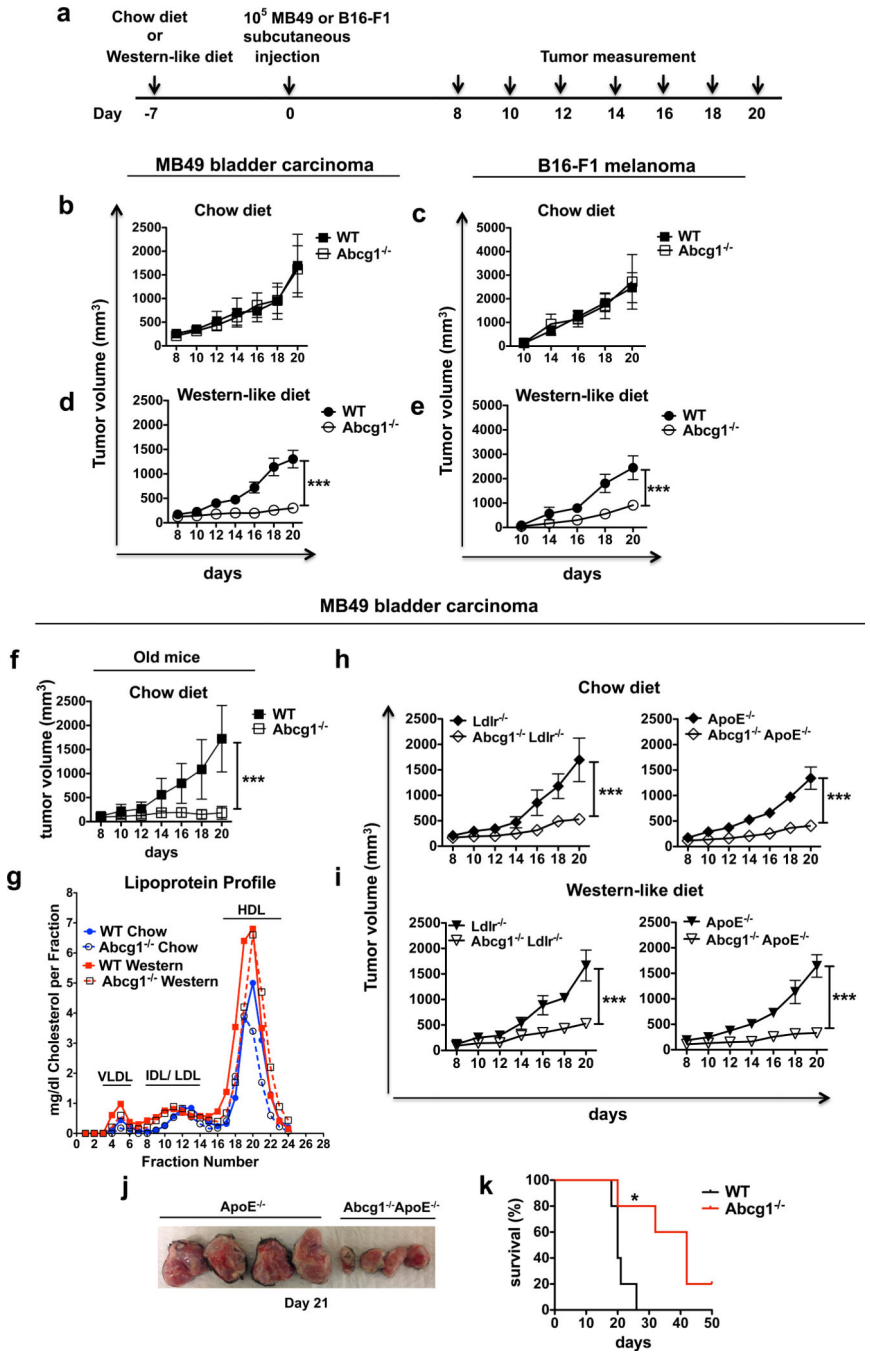

Figure 1. ABCG1 deficiency reduces MB49 and B16 tumor growth

(**a**) Schematic diagram of the experimental design is shown. Graphs show (**b**) MB49 and (**c**) B16F1 tumor growth in chow diet-fed and (**d**) MB49 and (**e**) B16F1 tumor growth in Western-like diet-fed 7–10 weeks old *Abcg1*$^{-/-}$ (*n*=8) and C57BL/6 (WT) mice (*n*=8) and (**f**) MB49 tumor growth in chow diet-fed 6–7 months old *Abcg1*$^{-/-}$ (*n*=6) and WT (*n*=7) mice. (**g**) Blood plasma from 5 tumor-bearing mice for each group was pooled and lipoprotein profile was analyzed by FPLC. Graph shows VLDL, IDL/LDL and HDL levels in all groups. (**h–j**) Graphs show MB49 tumor growth in (**h**) chow diet-fed and (**i**) Western-

like diet-fed *Abcg1*$^{-/-}$*Ldlr*$^{-/-}$ (*n*=6), *Ldlr*$^{-/-}$ (*n*=5); *Abcg1*$^{-/-}$*ApoE*$^{-/-}$ (*n*=8) and *ApoE*$^{-/-}$ (*n*=8) mice. (**j**) Picture shows harvested tumor masses from Western-like diet-fed *Abcg1*$^{-/-}$*ApoE*$^{-/-}$ and *ApoE*$^{-/-}$ mice at day 21. Data are representative of 2–4 independent experiments with similar results. (mean ± s.e.m., ***P< 0.001, two-way ANOVA test). (**k**) Graph shows Kaplan-Meier survival curve of Western-like diet-fed tumor (MB49) bearing *Abcg1*$^{-/-}$ (*n*=5) and WT mice (*n*=5). Data is representative of 2 independent experiments with similar results (mean ± s.e.m., *P< 0.05, log-rank test).

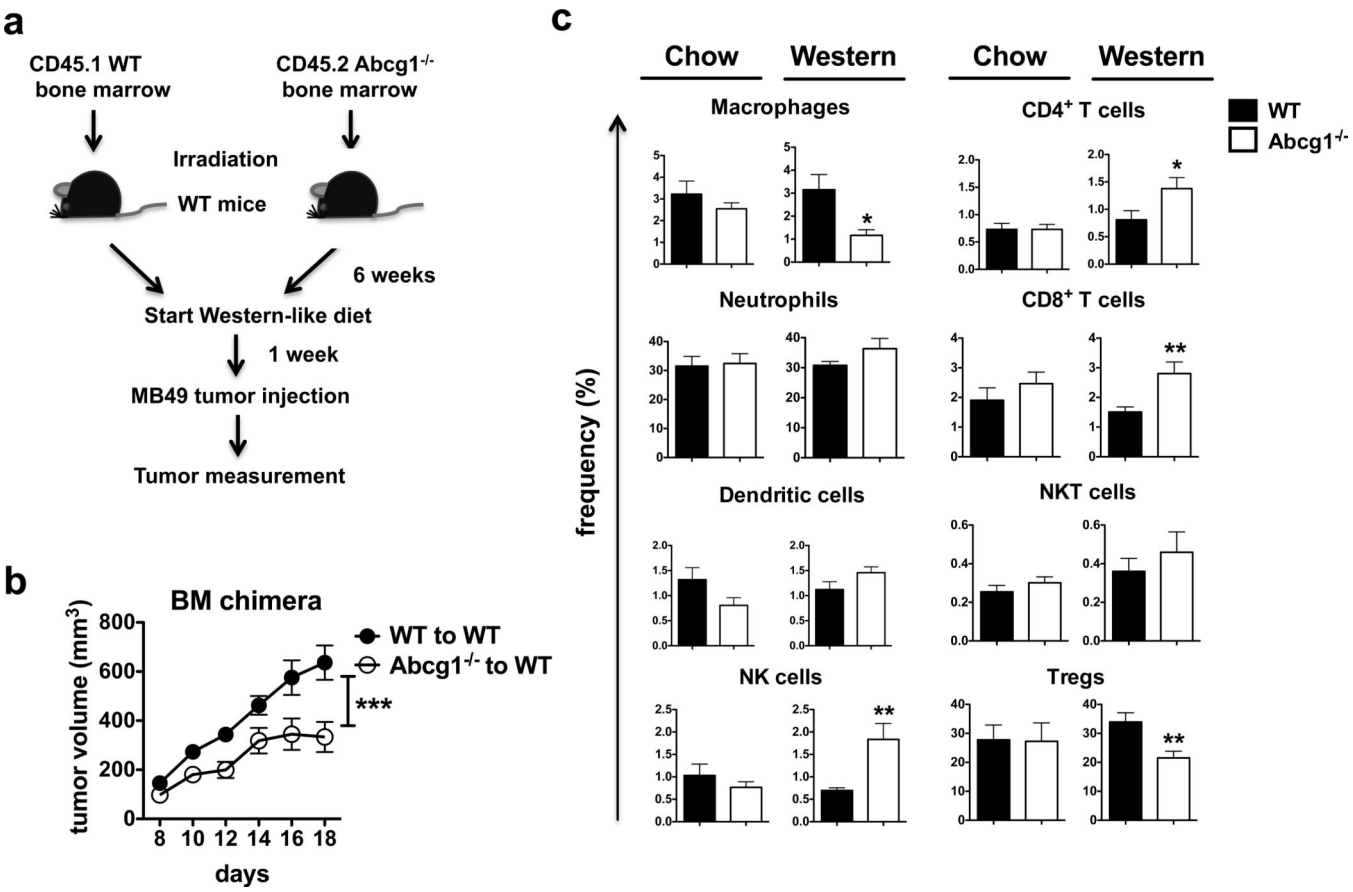

Figure 2. Impact of ABCG1 deficiency on tumor growth is immune cell-mediated

(**a,b**) Bone marrow chimeras were generated by reconstituting irradiated B6.SJL mice (*n* = 16 total) with bone marrow cells from CD45.1^{+} B6.SJL (WT) or CD45.2^{+} *Abcg1*$^{-/-}$ donor mice. (**a**) Schematic diagram of the experimental design is shown. (**b**) Graph shows MB49 tumor growth in the chimeric mice. Data is representative of 2 independent experiments with similar results (***P< 0.001, two-way ANOVA test). (**c**) Tumor cells from *Abcg1*$^{-/-}$ and C57BL/6 (WT) mice (*n*=5–7 per group) was analyzed by flow cytometry 20 days after injection of MB49 cells. Bar graphs show the frequencies of macrophages, neutrophils, dendritic cells, NK cells, CD4^{+} T cells, CD8^{+} T cells, NKT cells (% of live cells); and Tregs (% of CD4^{+} T cells) in the tumor. (See methods and Supplementary Fig. 2 for gating strategies). Data are pooled from 2 independent experiments with similar results (mean ± s.e.m., P< 0.05, **P < 0.01, two-tailed Student's t test).

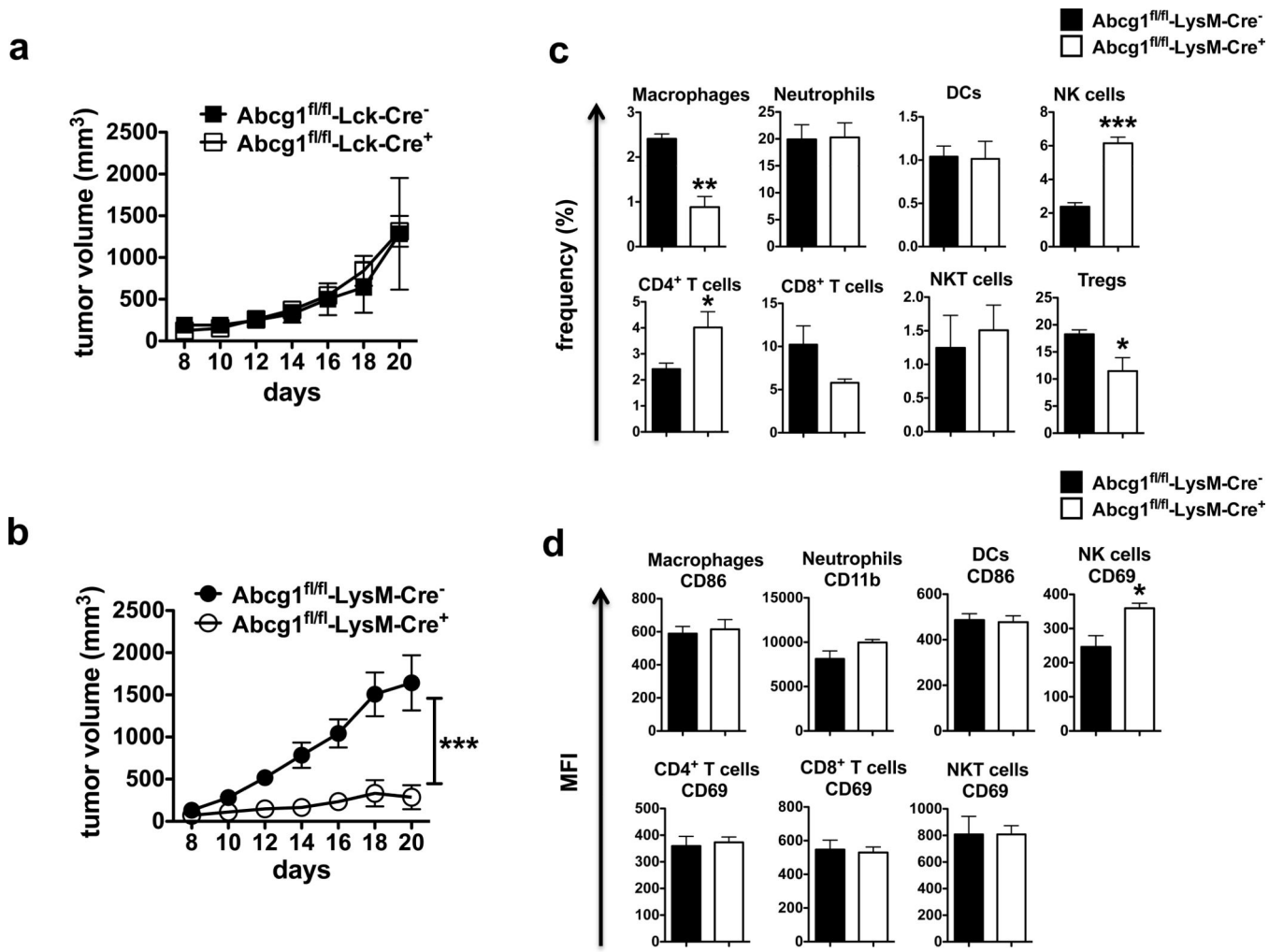

Figure 3. Reduced tumor growth in *Abcg1*$^{-/-}$ mice is myeloid cell-intrinsic

Graphs show MB49 tumor growth in Western-like diet-fed (**a**) Abcg1$^{fl/fl}$-Lck-Cre^{+} (*n*=7) and Abcg1$^{fl/fl}$-Lck-Cre^{-} (*n*=6) mice, (**b**) Abcg1$^{fl/fl}$-LysM-Cre^{+} (*n*=5) and Abcg1$^{fl/fl}$-LysM-Cre^{-} (*n*=7) mice. Data are representative of 2 independent experiments with similar results (***P< 0.001, two-way ANOVA test). Tumor cells from Western-like diet-fed Abcg1$^{fl/fl}$-LysM-Cre^{+} (*n*=5) and Abcg1$^{fl/fl}$-LysM-Cre^{-} mice (*n*=5) were analyzed by flow cytometry 20 days after injection of MB49 cells. (**c**) Bar graphs show the frequencies of macrophages, neutrophils, DCs, NK cells, CD4^{+} T cells, CD8^{+} T cells, NKT cells (% of live cells); and Tregs (% of CD4^{+} T cells) in tumor (See methods and Supplementary Fig. 2 for gating strategies). (**d**) Bar graphs show the MFI of indicated activation markers on immune cells in tumor. Data are representative of 2 independent experiments with similar results (mean ± s.e.m., *P < 0.05, **P < 0.01, ***P < 0.001, two-tailed Student's t test).

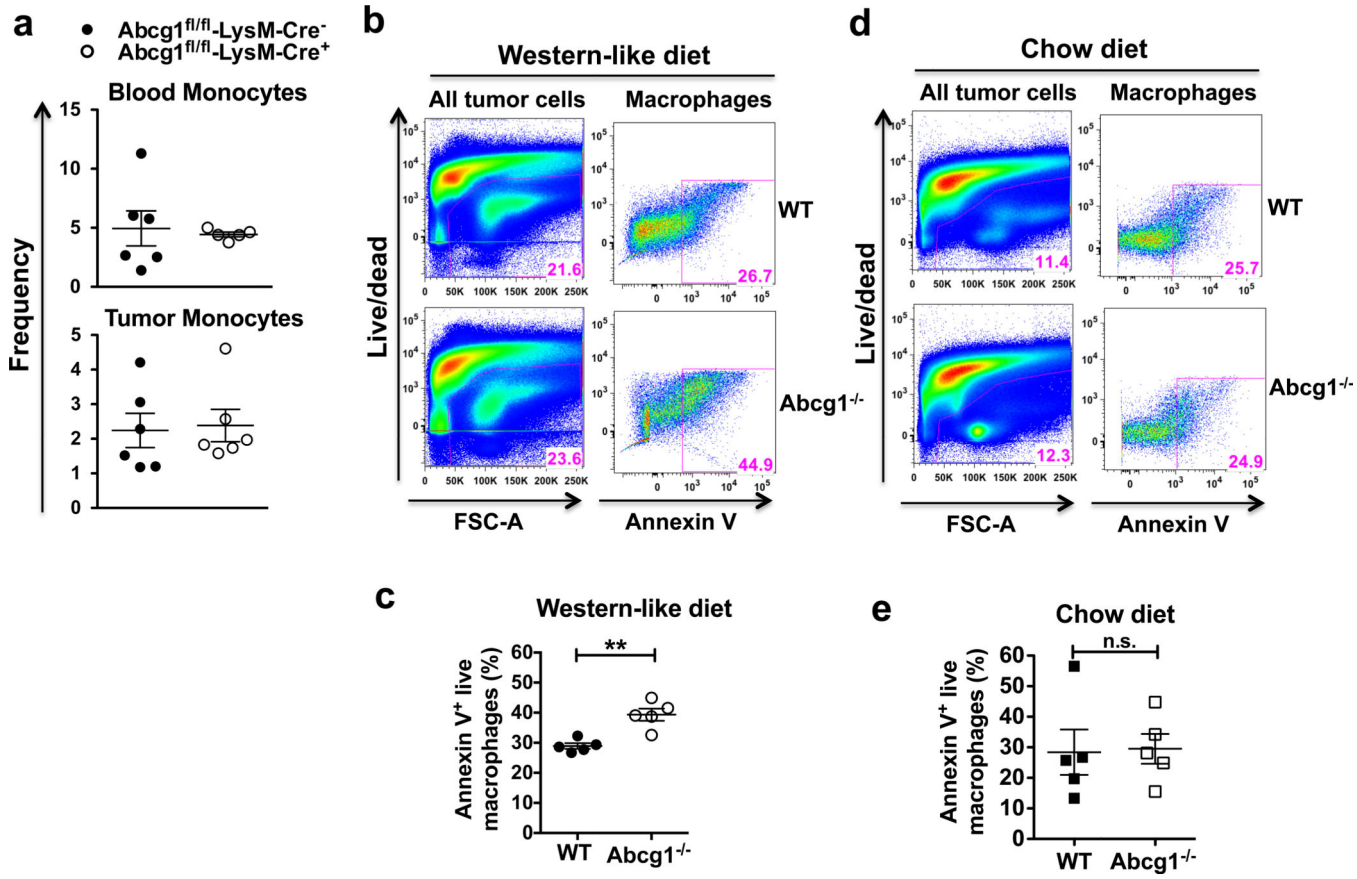

Figure 4. *Abcg1*$^{-/-}$ macrophages in the tumor display enhanced apoptosis under Western-like diet conditions

(**a**) Blood and tumor cells from Western-like diet-fed *Abcg1*$^{fl/fl}$-LysM-Cre^{+} (*n*=6) and *Abcg1*$^{fl/fl}$-LysM-Cre^{-} (*n*=6) mice were analyzed by flow cytometry 18 days after MB49 tumor injection. Dot plots show frequencies of monocytes (CD45^{+}, NK1.1^{-}, Ly6G^{-}, CD11b^{+}, CD115^{+}) (% of live cells) in blood (top) and tumor (bottom). (**b–e**) Tumor cells from *Abcg1*$^{-/-}$ (*n*=5) and WT (*n*=5) mice were analyzed for apoptosis by Annexin V staining and flow cytometry 12 days after injection of MB49 cells. **(b,d)** Representative pseudo-color plots show percentages of all tumor cells gated on live cells (left) and CD45^{+}, NK1.1^{-}, Ly6G^{-}, CD11b^{+}, F4/80^{high} macrophages, which are Annexin V^{+} (right). Dot plots show percentages of apoptotic (Annexin V^{+} live) macrophages in tumor from (**c**) Western-like-diet-fed and (**e**) chow diet-fed mice. Data are representative of 2 independent experiments with similar results (mean ± s.e.m., $^{**}P < 0.01$, two-tailed Student's t test).

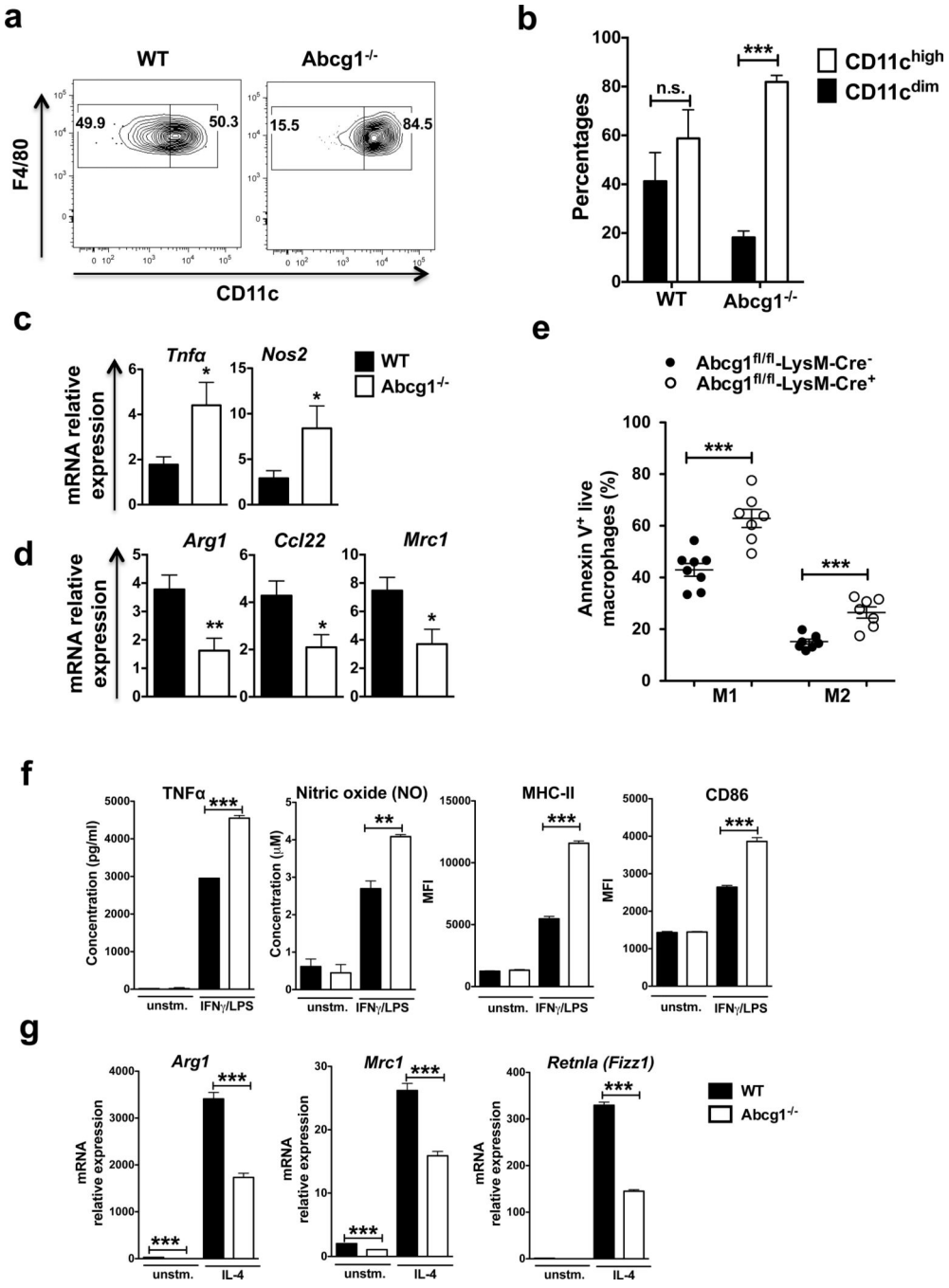

Figure 5. *Abcg1*$^{-/-}$ macrophages shift towards an M1 phenotype in the tumor

(**a,b**) Tumor cells from Western-like diet-fed *Abcg1*$^{-/-}$ (*n*=6) and WT mice (*n*=6) mice were analyzed by flow cytometry 20 days after injection of MB49 cells. (**a**) Representative contour plots and bar graphs show percentages of CD11c^{high} (M1-like) and CD11c^{dim} (M2-like) macrophages (CD45^{+}, NK1.1^{-}, Ly6G^{-}, CD11b^{+}, F4/80^{high}) in the tumor. (**c,d**) Macrophages were FACS-sorted from tumors from Western-like diet-fed *Abcg1*$^{-/-}$ and WT mice 20 days after inoculation of MB49 cells. Expression of (**c**) M1 markers *Tnfα* and *Nos2* and (**d**) M2 markers *Arg1*, *Ccl22*, *Mrc1* were measured by qPCR. (**e**) Tumor cells from

Western-like diet-fed *Abcg1*$^{fl/fl}$-LysM-Cre^{+} (*n*=7) and *Abcg1*$^{fl/fl}$-LysM-Cre^{-} (*n*=8) mice were analyzed for apoptosis by Annexin V staining and flow cytometry 12 days after injection of MB49 cells. Dot plot shows percentages of apoptotic (Annexin V^{+} live) M1 (CD11c^{high}) and M2 (CD11c^{dim}) macrophages in the tumor. Data are pooled from 2 independent experiments with similar results. (**f,g**) WT and *Abcg1*$^{-/-}$ BMDMs were polarized to an M1 phenotype by IFNγ/LPS stimulation or to an M2 phenotype by IL-4 stimulation, *in vitro*. Expression of (**f**) M1 markers and (**g**) M2 markers were analyzed by ELISA (TNFα), Griess reagent system (NO), flow cytometry (MHC-II, CD86) or qPCR (*Arg1, Mrc1, Retnla).* Data are representative of 2 independent experiments with similar results (mean ± s.e.m., **P* < 0.05, ***P* < 0.01, ****P* < 0.001, two-tailed Student's t test).

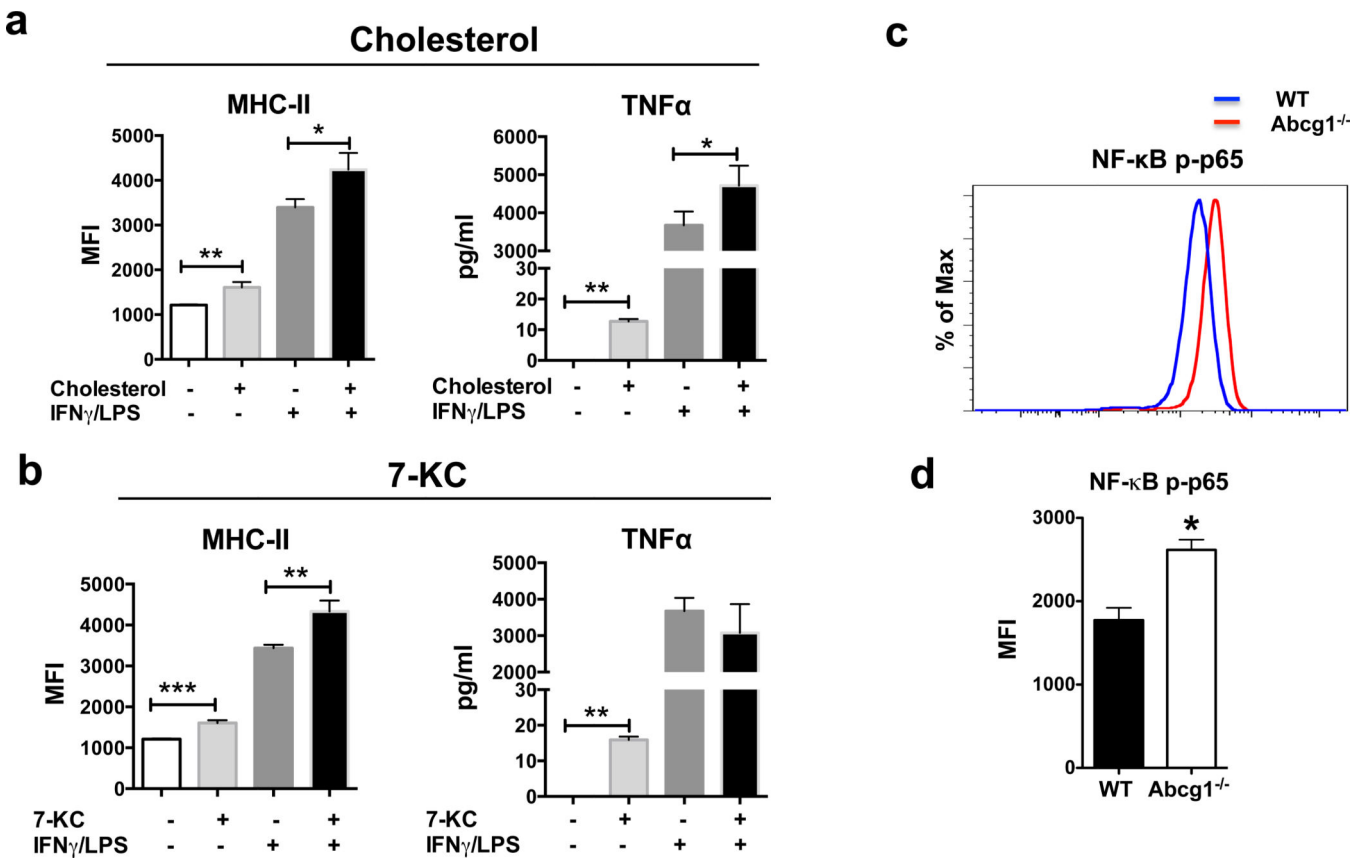

Figure 6. Cholesterol and 7-KC stimulation increase expression of M1 markers in macrophages

(a,b) WT bone marrow-derived macrophages were pre-incubated with cholesterol (20 μg/ml) or 7-KC (5 μM) for 2 hours. After that, the cells were stimulated with IFNγ (20 ng/ml) and LPS (100 ng/ml) or left unstimulated as described in the Methods. MHC II expression was analyzed by flow cytometry and TNFα production was analyzed by ELISA. (**c**) Representative plot and (**d**) graph show levels of NF-κB p65 phosphorylation (Ser 529) in *Abcg1*$^{-/-}$ and WT BMDMs analyzed by flow cytometry. Data are representative of 2 independent experiments with similar results. (mean ± s.e.m., **P* < 0.05, ***P* < 0.01, ****P* < 0.001, two-tailed Student's t test).

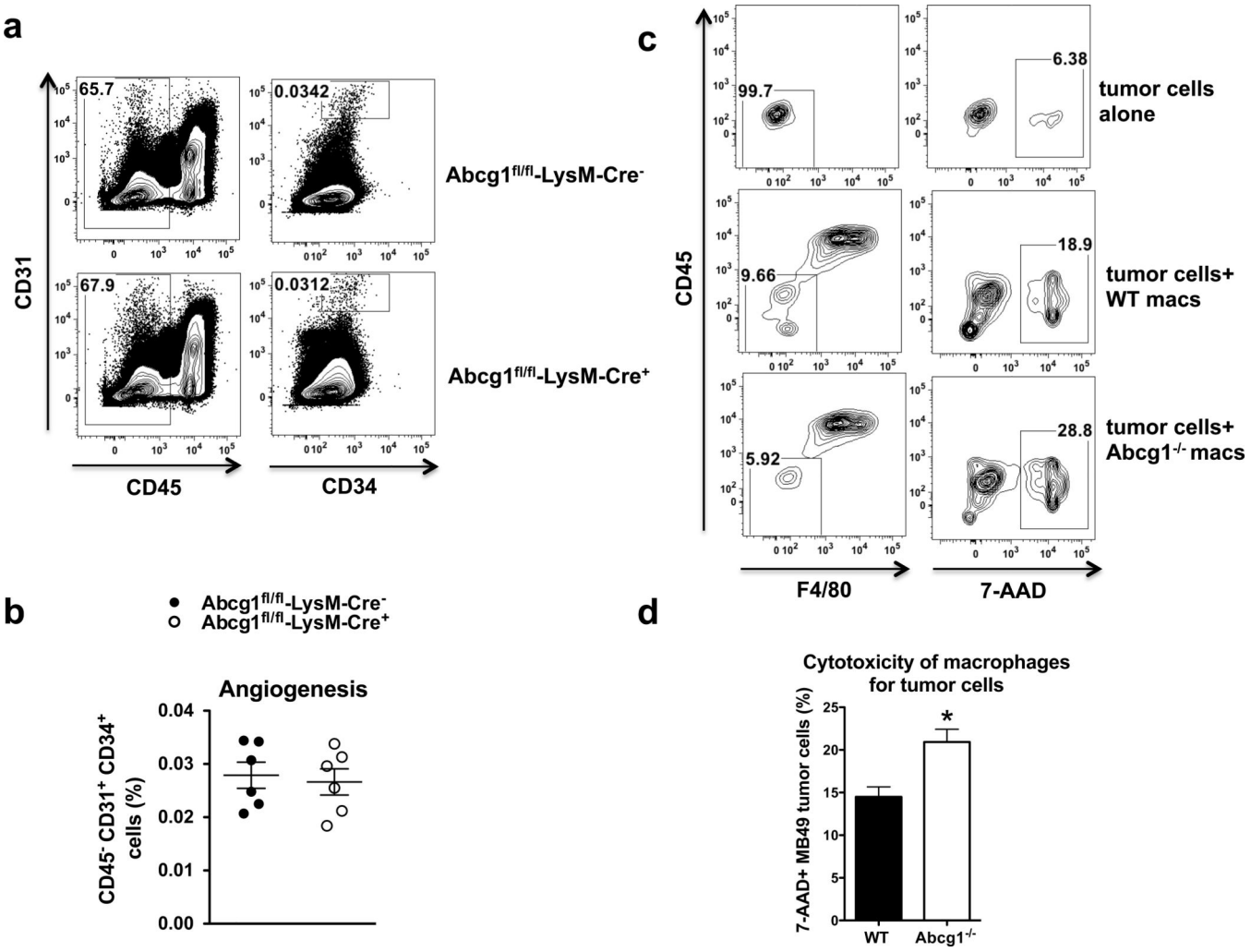

Figure 7. *Abcg1*$^{-/-}$ macrophages display enhanced cytotoxicity for tumor cells

(**a,b**) Tumor cells from Western-like diet-fed *Abcg1*$^{fl/fl}$-LysM-Cre^{+} (*n*=6) and *Abcg1*$^{fl/fl}$-LysM-Cre^{-} (*n*=6) mice were analyzed for angiogenesis markers by flow cytometry 18 days after injection of MB49 cells. (**a**) Representative contour plots and (**b**) dot plot show percentages of CD45^{-}, CD31^{+},CD34^{+} vascular endothelial cells in the tumor. (**c,d**) Cytotoxicity of macrophages for tumor cells was analyzed by flow cytometry (See methods). (**c**) Representative contour plots and (**d**) bar graph show percentages of CD45^{-}, F4/80^{-}, 7-AAD^{+} MB49 tumor cells. Data are representative of 2 independent experiments with similar results (mean ± s.e.m., **P* < 0.05, two-tailed Student's t test).